Alma Mater Studiorum · University of Bologna

School of Science
Department of Physics and Astronomy
Master Degree in Physics

PRIMORDIAL BLACK HOLES PRODUCTION IN HIGGS INFLATION

Supervisor:

Prof. Roberto Casadio

Submitted by:

Ilaria Carpi

Co-supervisor:

Dr. Alessandro Tronconi

Academic Year 2024/2025

Abstract

The current observational data deriving from the CMB and large-scale structures only probes a limited range of cosmological scales, hence the majority of the inflationary dynamics is still unconstrained. It is possible that processes of cosmological relevance, such as the generation of dark matter, occurred during these unobserved stages. In this context, primordial black holes (PBHs) represent an interesting dark matter candidate.

Higgs inflation is an interesting framework in which such phenomena may occur. Quantum corrections can flatten the effective potential in localized regions and induce an inflection point, leading to a temporary violation of the slow-roll conditions and to a transient phase of ultra–slow–roll. This phase amplifies the curvature perturbation spectrum on scales smaller than CMB scales, potentially triggering PBH formation at the end of inflation.

This thesis presents a Higgs inflation model that includes higher–order operators in both the scalar potential and the non–minimal coupling, ensuring compatibility with CMB observations while allowing for a significant enhancement of the power spectrum at smaller scales. The enhancement is obtained by means of a quasi-inflection point in the Einstein frame potential, and the parameter space of the model is compatible with the current bounds on the value of the Higgs quartic self-coupling λ. The resulting mass and abundance of the produced PBHs are evaluated by means of a numerical analysis and compared with current observational bounds.

Contents

Introduction

Since its introduction in the 1980s, following the fundamental works of A. Guth, A. Starobinsky and A. Linde [1, 2], inflation has become a cornerstone of modern cosmology. Nowadays, it is widely accepted as the most successful theoretical framework for describing the evolution of the Early Universe. Indeed, over the years, the inflationary paradigm has consistently provided accurate predictions for the anisotropies of the Cosmic Microwave Background (CMB) and the formation of large-scale structures (LSS), such as galaxy clusters, which are observable in the present Universe. Nevertheless, the current experiments only probe the largest cosmological scales, namely the region $10^{-4} \lesssim k[\mathrm{Mpc}]^{-1} \lesssim 10^{-1}$. This interval corresponds to only a small fraction of the early stages of the inflationary dynamics, therefore the vast majority of the inflationary period remains observationally unconstrained and may be characterized by dynamics that is not described by standard slow-roll models. In particular, it is possible that, during these unprobed phases, relevant phenomena, such as the generation of dark matter, may have occurred.

The origin of dark matter represents one of the major open problems in contemporary cosmology. Approximately $\sim 25\%$ of the total energy density of the present Universe is in the form of dark matter, yet its nature remains unknown. Among the possible scenarios, an intriguing possibility is that a fraction, or possibly the totality, of dark matter is composed of primordial black holes (PBHs). Primordial black holes are cosmological objects that form in the early Universe as a consequence of the gravitational collapse of density fluctuations of primordial origin, and other subsequent processes such as clustering and accretion. The interest in PBHs as dark matter candidates dates back to the 1970s with the pioneering work of Carr and Hawking [3, 4]. During the 1990s, the MACHO, EROS and OGLE experiments investigated micro-lensing events in our galaxy, suggesting that a small fraction of matter in our galaxy could consist of sub-solar mass PBHs. More recently, the detection of gravitational waves from black-hole mergers by the LIGO/VIRGO collaboration has further increased interest in these objects, as it has been proposed that some of these signals could originate from the coalescence of PBHs.

The formation of primordial black holes requires the presence of regions in which the primordial density contrast exceeds a critical threshold δ_c. Once this condition is satisfied,

the overdense region collapses onto itself, leading to the formation of a PBH. The density perturbations responsible for PBH formation originate from quantum fluctuations, generated during inflation. These quantum fluctuations are stretched to super-Hubble scales during inflation, and in this peeriod they evolve classically according to the inflationary dynamics. When these perturbations re-enter the horizon at late times, they result in density fluctuations. The spectrum of such fluctuations depends entirely on the dynamics of inflation, which in turn is determined by the inflation action. This action varies from model to model.

In this thesis, we consider the case in which the inflaton is identified with the Higgs field. This scenario provides an economical and theoretically appealing framework, as it does not require the introduction of scalar fields beyond the Standard Model.

Higgs inflation requires a non-minimal coupling between the Higgs field and the Ricci scalar. The presence of this term is motivated since the quantum corrections on the dynamics of a scalar field on curved background are known to generate this contribution. The generation of PBHs in this context requires a temporary violation of the standard slow-roll conditions, which can be obtained by introducing features in the scalar potential that lead to a transient ultra-slow-roll phase. In particular, it is assumed that the effective potential exhibits an (exact or quasi) inflection point, at which the potential becomes significantly flatter than in the surrounding regions. After a brief introduction on the original Higgs inflation scenario, we study the influence of this ultra-slow-roll phase on the curvature perturbations in the context of an effective field theory valid at inflationary energy scales, with the aim of determining the resulting PBH mass spectrum and abundance.

This thesis is organised as follows:

1. Chapter 1 provides an overview of the Big Bang model (that describes the Universe at the present time) and its limitations, and introduces the inflationary paradigm as a solution to these shortcomings. The explanation of the CMB anisotropies within the inflationary framework is discussed in detail.

2. In Chapter 2 we study the theory of quantum perturbations generated during inflation. Starting from the dynamics of the inflaton, the expressions for the power spectra of scalar and tensor perturbations are derived, as well as the expressions of other important observable quantities (scalar spectral index and tensor-to-scalar ratio), and we review some general amplification mechanisms capable of modifying such spectra.

3. Chapter 3 introduces the physics of primordial black hole formation. In particular, we discuss the conditions required for PBHs production, together with the current relevant observational constraints and astrophysical bounds on the mass and abundance of PBHs.

4. In Chapter 4 we present the concept of Jordan frame, focusing on the transformation between the Jordan and Einstein frames. The relevant frame transformation formulas are derived, and the criteria for different inflationary regimes in the two frames are specified, focusing in particular on the slow-roll and ultra-slow-roll regimes.

5. Chapter 5 introduces the original model of Higgs inflation proposed by Bezrukov and Shaposhnikov [5, 6] and then discusses one of its possible extensions, the critical Higgs inflation scenario, in which an inflection point is introduced in the effective potential. An original Higgs inflation model, including higher-dimensional operators in the potential and in the non-minimal coupling to gravity, is then constructed and analysed numerically. The enhancement of the curvature perturbation spectrum, due to the presence of a quasi-inflection point, is investigated for different choices of model parameters, and the resulting mass and abundance of PBHs are computed.

Chapter 1

Introduction on inflation

In this introductory chapter, we will illustrate some basic concepts of modern cosmology, such as FLRW spacetime and the Universe dynamics, to then explain the theory of inflation and the motivations behind it.

1.1 Friedmann-Robertson-Walker spacetime

Cosmological models that describe the current state of the Universe are based on the fundamental assumption, backed up by experimental evidence throughout the years, that our Universe is homogeneous and isotropic. In this context, homogeneity means that the Universe's density is the same in every point in spacetime, while isotropy equals the concept of the Copernican principle, according to which the Universe appears to have the same properties regardless of which point it is observed from.

According to these assumptions, the general form of a spacetime metric describing our Universe is the Friedmann-Lemaitre-Robertson-Walker metric (FLRW):

$$ds^2 = -dt^2 + a^2(t)\left(\frac{dr^2}{1-kr^2} + r^2(d\theta^2 + sin^2\theta d\varphi^2)\right) \tag{1.1.1}$$

The constant k fixes the Universe's constant-t hypersurfaces' curvature as flat ($k = 0$), open ($k = 1$) or closed ($k = -1$). Current observations on the CMB seem to suggest that our Universe is flat, so $k = 0$. The other important element is the scale factor $a(t)$, which represents the relative size of constant-t hypersurfaces.

An important quantity that characterizes the evolution of the Universe is the Hubble parameter, defined as:

$$H = \frac{\dot{a}(t)}{a(t)} \tag{1.1.2}$$

In particular, the inverse of $H(t)$ sets some fundamental time and length scales of the

Universe's spacetime.

1.2 Universe dynamics

By solving Einstein equations in the FLRW spacetime (1.1.1), one obtains the Friedmann equations, which describe the evolution of a given cosmological model in the FLRW metric. Usually, it is assumed that the Universe is filled with a perfect fluid having the following stress-energy tensor:

$$T^{\mu}{}_{\nu} = \begin{pmatrix} -\rho & 0 & 0 & 0 \\ 0 & p & 0 & 0 \\ 0 & 0 & p & 0 \\ 0 & 0 & 0 & p \end{pmatrix} \tag{1.2.1}$$

In this expression, ρ is the energy density and p represents the pressure. The Friedmann equations are:

$$H^2 = \left(\frac{\dot{a}}{a}\right)^2 = \frac{\rho}{3} - \frac{k}{a^2} \tag{1.2.2}$$

$$\dot{H} + H^2 = \frac{\ddot{a}}{a} = -\frac{\rho + 3p}{6} \tag{1.2.3}$$

These two equations are coupled, since the matter content satisfies the continuity equation:

$$\dot{\rho} = -3H(\rho + p) \tag{1.2.4}$$

The energy density and pressure of a perfect fluid follow the equation of state

$$p = \omega\rho \tag{1.2.5}$$

where the factor ω is different for each type of content: $\omega = 0$ for dust (weakly-interacting matter), $\omega = 1/3$ for radiation, and $\omega = -1$ for the cosmological constant $H_\lambda = \sqrt{\lambda/3}$ which can be originated by the quantum vacuum energy. This latter component is responsible for the current expansion of the Universe, revealed mainly by observing cosmological objects traveling away from each other.

To give another insight on the cosmological model that we are describing, the equation (1.2.2) can be rewritten in the following way:

$$1 - \Omega(a) = -\frac{k}{(aH)^2} \ . \tag{1.2.6}$$

The quantity $\Omega(a) = \frac{\rho}{\rho_{crit}}$ is a relative density, where ρ_{crit} is the value of density that

corresponds to a flat Universe (to $k = 0$, according to Eq. (1.2.6)). This form of the equation is useful to understand the evolution of the density value and its relation to the Universe's spatial curvature k. In particular Eq. (1.2.6) indicates that, in an expanding universe with dust and radiation, $1 - \Omega(a)$ increases as a increases.

1.3 Strong energy condition

The strong energy condition

$$\rho + 3p \geq 0 \tag{1.3.1}$$

is a property of ordinary matter in the Universe, as opposed to cosmological constant content. For cosmological fluids, this has an important implication. Indeed, by looking at Eq. (1.2.3), it is evident that, if the strong energy condition is valid, the acceleration of the scale factor has to be negative, because the scale factor $a(t)$ is defined to be positive at any time. This means that, if the Universe is filled with either matter or dust, its expansion is slowing down as it expands.

In the case of cosmological constant, the equation of state is $p = -\rho$, which means that the strong energy condition is violated, so the Universe filled with cosmological constant undergoes accelerated expansion.

1.4 ΛCDM model

The picture of the current state of the Universe is commonly considered the ΛCDM model, that describes it as spatially flat ($k = 0$), with an average density today:

$$\rho_0 = \rho_{crit} \simeq 10^{-29} g/cm^3 \,. \tag{1.4.1}$$

Contributions to this density come from four different sources:

1. Standard Model (SM) matter: $\frac{\rho_{matter}}{\rho_0} \simeq 5\%$
2. Dark matter (DM): $\frac{\rho_{dm}}{\rho_0} \simeq 25\%$
3. Dark energy: $\frac{\rho_{de}}{\rho_0} \simeq 70\%$
4. Radiation: $\frac{\rho_r}{\rho_0} \ll 1\%$

The nature of dark matter and dark energy are two of the biggest puzzles in the current cosmology landscape. Indeed, PBHs could explain a part of, if not all of, the DM content present in the Universe, without invoking new physics beyond the Standard Model. This

is the main reason for which the topic of PBH formation is of significant interest in modern cosmology.

1.5 Horizon and flatness problem

The standard cosmology picture of the ΛCDM Universe holds quite well in light of current experimental results; however, it unfortunately has some shortcomings when it comes to the primordial Universe. To illustrate them, it is necessary to introduce the concept of a particle horizon and its importance in the causal structure of the Universe.

Starting from the current Universe state and going back in the time coordinate, the ΛCDM model predicts the presence of a singularity, that can be referred to as the Big Bang, at a time that can be set to $t = 0$, when the scale factor is $a(0) = 0$. By taking the radial null trajectories in FLRW spacetime:

$$dr = \frac{dt}{a(t)} \tag{1.5.1}$$

and integrating from $t = 0$, which corresponds to $r = 0$, to the present time, we obtain the comoving radial coordinate travelled by light particles from the Big Bang, and by multiplying this quantity by $a(t)$ we obtain the so-called particle horizon:

$$r_p = a(t) \int_0^t \frac{dt}{a(t)} \, . \tag{1.5.2}$$

The particle horizon can also be written as the integral over a quantity called comoving Hubble radius $1/aH$:

$$r_p = \int_0^a \frac{d \ln a}{aH} \, . \tag{1.5.3}$$

The two quantities are proportional. Indeed, considering the evolution of the Hubble parameter with respect to a in a Universe filled with a generic cosmological fluid, $H = H_0(a_0/a)^n$, the integral above gives the following result:

$$\int_{a_0}^{a} \frac{\mathrm{d}a}{a^2 H} = \int \mathrm{d}a \frac{a^{n-2}}{H_0 a_0^n} = \left(\frac{1}{n-1}\right) \frac{a^{n-1}}{H_0 a_0^n} = \left(\frac{1}{n-1}\right) \frac{1}{aH} \tag{1.5.4}$$

The comoving Hubble radius approximately sets the scale for regions in the Universe in which all points are in causal contact at a given instant in time, as it roughly coincides with the particle horizon, which represents the maximum distance between two points for them to *have been* in causal contact at some time in the Universe history. Regions of the Universe that are separated by a distance greater than r_p could have never been in

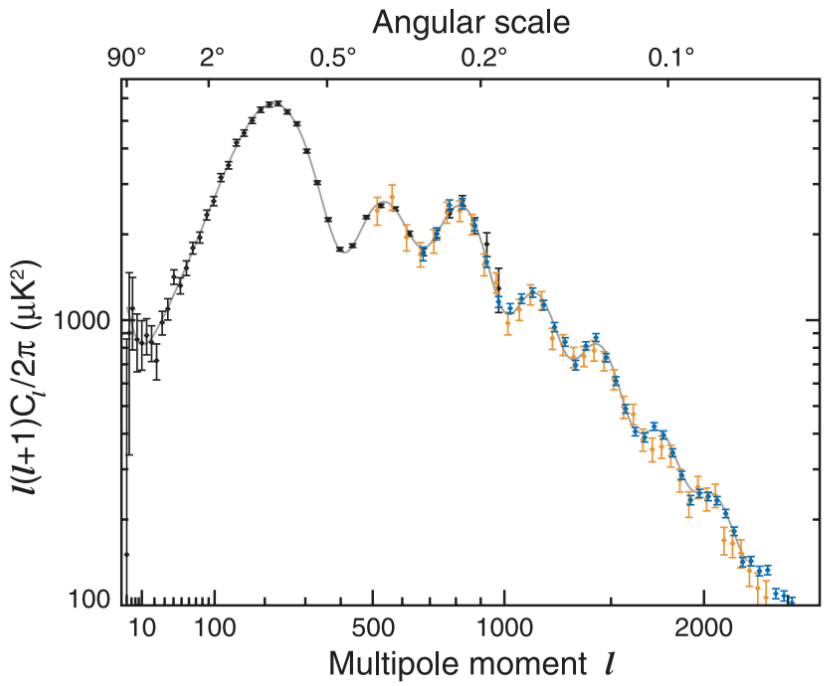

Figure 1.1: CMB fluctuations measured in multipole moments [7]

causal contact with each other in the Big Bang picture.

In 1964, the Cosmic Microwave Background signal was measured for the first time [8]. This signal is the residual radiation from an event called recombination, the moment in the Early Universe when radiation decoupled to matter, leaving behind a spectrum of high energy photons. The peculiar feature of the CMB spectrum that is currently observed is its isotropy. In fact, this spectrum appears to have an average temperature $T_{cmb} = 2.725$ K, and deviations from this temperature are very small, regardless of the directions of the photons. This is illustrated in Fig. (1.1) from [7], where it is clear that CMB spectrum fluctuations are very small (the scale is μK) at all observed angular scales (the multipole moment l is inversely proportional to the length scale of the fluctuation). The CMB fluctuations carry two shortcomings of the standard Big Bang cosmology model:

1. **Horizon problem**: according to the Big Bang picture, if we take two points in the sky, whose distance is greater than the particle horizon r_s, these will belong to two regions which were causally disconnected at the time of recombination. So, the question about how it is possible that the CMB radiation is so smooth, given that many points from which we make correlation measurements were never put in causal contact with each other before arises.

2. **Flatness problem**: as we have seen, the Universe appears to have a flat geometry, that, from Friedmann equation ((1.2.6)), corresponds to $\Omega(a) \simeq 1$. Since $\Omega(a) - 1$ increases in an expanding Universe with dust and radiation, it must have been extremely close to zero immediately after the Big Bang.

1.6 Inflation as a solution

Inflation was first proposed in 1980 by Alan Guth [1]. In his article, it is stated that the inflationary paradigm could be the solution to both flatness and horizon problems, and throughout the years it has remained the most widely accepted theory for Early Universe physics.

The premise of inflation theory is that, before recombination, the Universe underwent a period of exponential expansion, when the Universe is in a state called a quasi-De Sitter state, with the Hubble parameter H having an almost constant value (De Sitter corresponds to constant H). During this period, the Universe is filled with some fluid which approximately behaves as the cosmological constant ($p = -\rho$), and the scale factor has the following evolution:

$$a(t) = e^{Ht} \tag{1.6.1}$$

In this scenario, the acceleration of the scale factor is positive, because:

$$\dot{H} = 0 \quad \Longrightarrow \quad \frac{\ddot{a}}{a} - H^2 = 0 \quad \Longrightarrow \quad \ddot{a} > 0 \tag{1.6.2}$$

This follows from the fact that $a(t)$ is always positive over time.

When the Universe expands exponentially, an important condition holds: the comoving Hubble radius shrinks (instead of expanding like it does in the presence of radiation or ordinary matter):

$$(aH)^{-1} = 1/\dot{a} \quad \Longrightarrow \quad \frac{d}{dt}(aH)^{-1} = -\frac{\ddot{a}}{\dot{a}^2} < 0 \tag{1.6.3}$$

The inflation mechanism then represents a possible solution to the aforementioned shortcomings of Big Bang theory because:

1. If the inflationary period lasts long enough, the comoving Hubble radius shrinks and allows for the existence of a time in the Early Universe in which the size of causal patches is much larger than what the Big Bang picture allows (Fig. (1.2)). In this way there is a point in the past in which all points in the Universe were actually in causal contact with each other, solving the smoothness problem of the CMB radiation.

2. Looking at Eq. (1.2.6), a shrinking comoving Hubble radius implies that the solution where $\Omega = 1$ is an attractor for an expanding universe with $\dot{H} \simeq 0$. This eliminates the need of fine tuning of initial conditions in the Early Universe to obtain flatness. Even during the cosmological evolution after inflation, Ω does not deviate from the critical value too much, so the flatness is preserved. The Universe

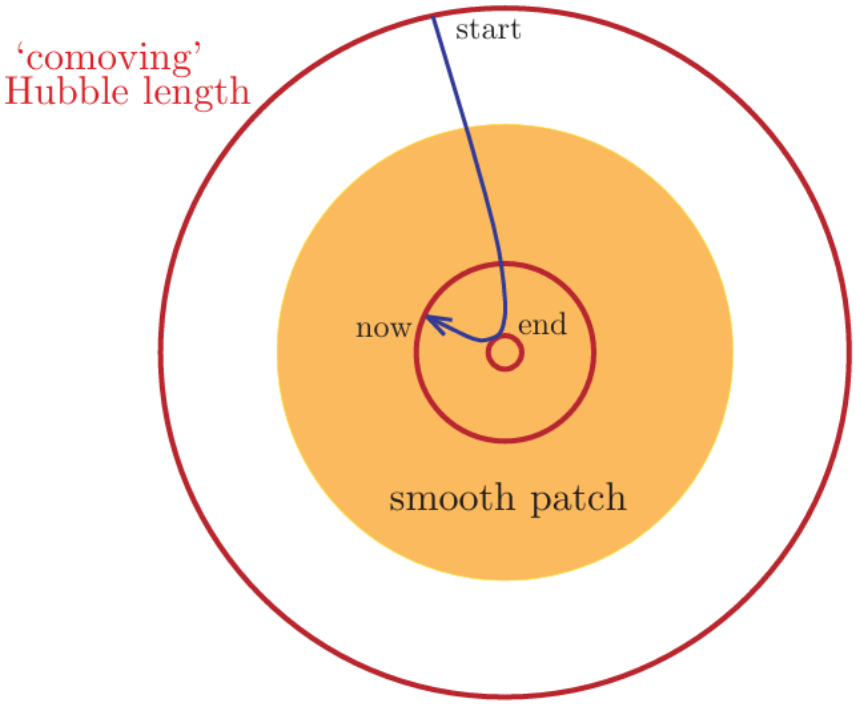

Figure 1.2: Change of the Hubble radius during inflationary era [9]

flatness is therefore also explained by inflation.

1.7 General characteristics of an inflationary theory

We have explained inflation theory premises, but how is it realized in practice? How do we motivate the presence of such a period in the Universe history? A well-motivated theory for the dynamics of inflation, that is robust against all experimental observations, has yet to be found. The most studied assumption is that inflation is driven by one scalar field, called the inflaton. The inflaton action can be added to the usual Einstein-Hilbert action as follows:

$$S_{infl} = S_{HE} + S_{\phi} = \int d^4x\sqrt{-g}\left[-\frac{M_P^2}{2}R + \partial_\mu\partial^\mu\phi - V(\phi)\right] . \tag{1.7.1}$$

By varying this action with respect to the metric, as usual we obtain the two Friedmann equations (1.2.2) and (1.2.3), which we can write in a form that is more suitable to study the inflaton dynamics:

$$H^2 = \frac{1}{3M_P^2}\left(\frac{\dot{\phi}^2}{2} + V(\phi)\right) , \tag{1.7.2}$$

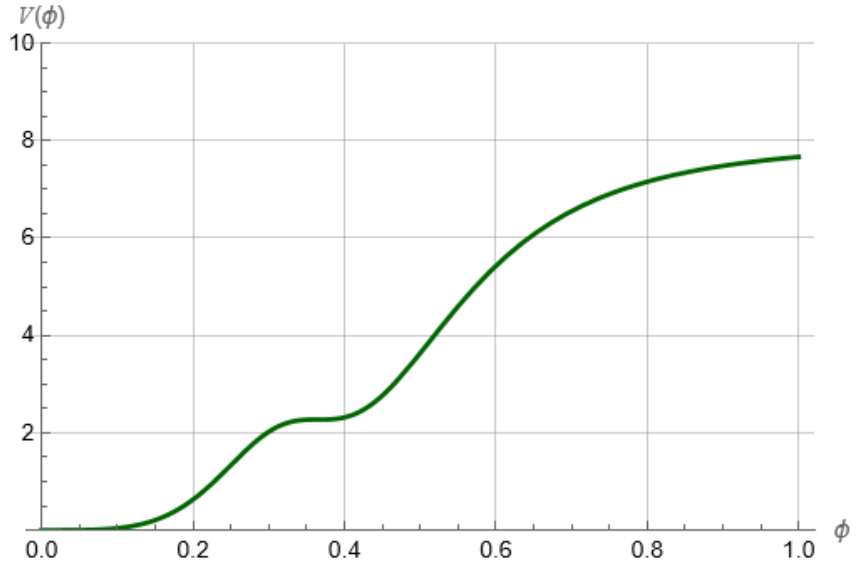

Figure 1.3: An example of potential for a possible inflation scenario.

$$\dot{H} = -\frac{1}{2M_P^2}\dot{\phi}^2 \,. \tag{1.7.3}$$

Then, by varying the action with respect to the field ϕ, we obtain the Klein-Gordon equation for the inflaton field:

$$\ddot{\phi} + 3H\dot{\phi} + V'(\phi) = 0 \,. \tag{1.7.4}$$

These three equations solved together determine the dynamics of inflation, that will generally depend on the form of the potential $V(\phi)$. The general idea is to take, at the start, the inflaton field to sit on top of a quasi-flat region of the inflation potential $V(\phi)$, with a very small initial velocity, then slowly roll down this plateau, and, at the end of inflation, fall into the true vacuum of the inflaton field. This regime is called slow-roll regime, and it is the most common mechanism employed to achieve inflation. A generic form for the inflaton potential is depicted in Fig. (1.3).

At a more formal level, the main requirement of inflation, which is the slow decrease of the Hubble radius, can be expressed as a condition on the so-called slow-roll parameter ε:

$$\varepsilon \equiv -\frac{\dot{H}}{H^2} \ll 1 \,. \tag{1.7.5}$$

Other slow-roll parameters can be defined, to describe the details of the inflaton motion. For example, in the slow-roll regime mentioned above, we could impose:

$$\delta \equiv -\frac{\ddot{\phi}}{H\dot{\phi}} \ll 1 \tag{1.7.6}$$

where the slow-roll parameter δ is related to the acceleration of the inflaton. The acceleration $\ddot{\phi}$ has to be small enough in order for inflation to last long enough to solve the horizon and the flatness problem. Other slow-roll parameters can be defined by further differentiating the Hubble parameter and the field and obtaining the so-called Hubble flow function hierarchy (starting from $\epsilon_0 = H_0/H$):

$$\epsilon_{i+1} = \frac{\dot{\epsilon_i}}{H\epsilon_i} \tag{1.7.7}$$

and the scalar field flow function hierarchy (starting from $\delta_0 = \phi/\phi_0$):

$$\delta_{i+1} = \frac{\dot{\delta_i}}{H\delta_i} \ . \tag{1.7.8}$$

Applying the conditions (**??**) the equations of the inflaton dynamics become:

$$H^2 \approx \frac{V(\phi)}{3M_P^2} \tag{1.7.9}$$

$$\dot{\phi} \approx -\frac{V'(\phi)}{3H} \tag{1.7.10}$$

1.8 Overview of inflationary models

Over the years, many models have been proposed in order to explain the dynamics of inflation. Here we will list the main models that are representatives of the wide range that has been studied in literature in the past years.

1.8.1 Large-field models

In large-field models, the inflaton spans a range of values that is comparable to the Planck mass order of magnitude, $\Delta\phi > M_P$. Remaining in the context of single-field inflation, a prototype of large-field inflation is chaotic inflation [10], where the potential is dominated by a term

$$V(\phi) = \lambda\, \phi^p \ . \tag{1.8.1}$$

In this type of model, the self-coupling has to be very small in order to prevent large density fluctuations that could disrupt the inflationary regime.

Another relevant model in this class is natural inflation [11], where the potential takes the form

$$V(\phi) = V_0 \left[\cos\left(\frac{\phi}{f}\right) + 1\right] \ . \tag{1.8.2}$$

In natural inflation the field is often taken to be an axion. Axions provide a shift symmetry that can be employed to protect the potential from large quantum corrections at large field values. The range of ϕ depends on the parameter f, indeed, the field can oscillate between 0 and $2\pi f$.

1.8.2 Small-field models

In small-field models, the field moves in a range that is smaller than the Planck mass, $\Delta\phi < M_P$, and these models are often linked to mechanisms of spontaneous symmetry breaking. An example of such models is Higgs inflation [6], where the potential has the form

$$V(\phi) = V_0 \left[1 - \left(\frac{\phi}{\mu}\right)^2\right]^2 . \tag{1.8.3}$$

Higgs inflation is interesting for its convenience, as it postulates that the Higgs boson could act also as the inflaton field. There are some variations to this model to accommodate also the possibility of primordial black holes production.

Another famous small-field model is the Coleman-Weinberg potential [2]

$$V(\phi) = V_0 \left[\left(\frac{\phi}{\mu}\right)^4 \left(\ln\left(\frac{\phi}{\mu}\right) - \frac{1}{4}\right) + \frac{1}{4}\right] . \tag{1.8.4}$$

This potential was initially linked to radiatively-induced symmetry breaking in electroweak and grand unified theories, and although in this context the parameters in the model cannot accommodate inflation, this potential remains a good phenomenological model.

1.8.3 Hybrid models

In hybrid models, the inflaton field evolves towards a minimum with non-zero vacuum energy, then a second field, called the auxiliary field, becomes unstable, causing the end of inflation. This setup frequently appears in models in which inflation is incorporated into supersymmetry or supergravity. An example of potential for hybrid inflation is [12]

$$V(\psi, \phi) = \frac{1}{4\lambda}(M^2 - \lambda\psi^2)^2 + \frac{m^2}{2}\phi^2 + \frac{g^2}{2}\phi^2\psi^2 . \tag{1.8.5}$$

Different potentials can belong to different physical contexts, depending on the parameters choice and the nature of the fields.

Chapter 2

Perturbations

Cosmological perturbations are a fundamental concept in cosmology, because they represent the contact point between theory and observations. In fact, what we observe from experiments (the large-scale structure of the Universe, the CMB radiation spectrum, gravitational waves and dark matter) is partially the product of the evolution over time of these perturbations. Cosmological perturbations are the link between the macroscopic observations of the Universe and the quantum field theory of the inflaton, that is why this is a very important area to study.

In this chapter, we will discuss in detail the generation and dynamics of cosmological perturbations, to then focus on the mechanisms that amplify the spectrum of perturbations. This part is important for the study of primordial black holes generation, which is the main focus of this thesis. The main references for this chapter are [13–16].

2.1 Generalities on perturbations

The main idea of the perturbation approach is to split physical quantities into two parts, one being the background, which evolves in cosmic time, and the other being the perturbation, which also depends on the space coordinates and is significantly smaller than the background. The generic expression of a perturbed quantity is:

$$Q(x,\tau) = \tilde{Q}(\tau) + \delta Q(x,\tau) \tag{2.1.1}$$

where Q can be the metric field $g_{\mu\nu}$ or any matter field. At linear order, expanding the Einstein equations, the background evolves independently from the perturbations, and the Einstein equations for the perturbations have the same form as the Einstein equations of the background:

$$\delta G_{\mu\nu} = 8\pi G\, \delta T_{\mu\nu} \ . \tag{2.1.2}$$

Being the Universe spatially flat, homogeneous and isotropic, there are symmetries that allow for a decomposition of the metric and matter perturbations into three types of components, called scalar, vector, and tensor perturbations, that evolve independently at linear level. This decomposition is called the SVT decomposition, where the three types are classified depending on their helicity. The helicity is a property that is defined starting from the Fourier transform of a perturbation

$$X_{\mathbf{k}}(t) = \int d^3\mathbf{x}\, X(t,\mathbf{x})\, e^{i\mathbf{k}\cdot\mathbf{x}} \tag{2.1.3}$$

which is characterized by a vector $\mathbf{k}$, and the helicity is defined according to how the perturbation behaves under a rotation of an angle θ around this vector. The amplitude of a perturbation will change by a factor $e^{im\theta}$, and m is the helicity. This number is 0 for scalar, ± 1 for vector and ± 2 for tensor perturbations.

The SVT decomposition is a useful formalism because each type of perturbation has different transformation properties and, because of the rotational invariance of the background, each perturbation evolves separately at linear level.

2.1.1 Metric perturbations

Metric perturbations originate from fluctuations of the metric field $g_{\mu\nu}$. The most general form for a spatially flat FLRW metric at first order in the perturbations is:

$$ds^2 = -(1+2\Phi)dt^2 + 2aB_i dx^i dt + a^2((1-2\Psi)\delta_{ij} + E_{ij})dx^i dx^j \tag{2.1.4}$$

where the perturbations are Φ, B_i, Ψ, E_{ij}. In particular, these can be further decomposed, according to the SVT decomposition, in the following components:

$$B_i \equiv \partial_i B - S_i \tag{2.1.5}$$

where $\partial^i S_i = 0$, and

$$E_{ij} \equiv 2\partial_{ij}E + 2\partial_{(i}F_{j)} + h_{ij} \tag{2.1.6}$$

where $\partial^i F_i = 0$ and h_{ij} is traceless. Scalars don't have indexes, vectors have one index and tensors have two.

2.1.2 Matter perturbations

During inflation, the matter perturbations come from the perturbed inflaton field. The perturbed stress energy tensor has the following components:

$$T_0^0 = -(\bar{\rho} + \delta\rho) \tag{2.1.7}$$

$$\tag{2.1.8}$$

$$T_i^0 = (\bar{\rho} + \bar{p})\, a v_i \tag{2.1.9}$$

$$\tag{2.1.10}$$

$$T_0^i = -(\bar{\rho} + \bar{p})\frac{(v^i - B^i)}{a} \tag{2.1.11}$$

$$\tag{2.1.12}$$

$$T_j^i = \delta_j^i(\bar{p} + \delta p) + \Sigma_j^i \ . \tag{2.1.13}$$

Perturbations $\delta\rho$ and δp are scalar, as well as the momentum density, defined with the relation

$$\partial_i(\delta q) = (\bar{\rho} + \bar{p})v_i \ . \tag{2.1.14}$$

Other perturbations are B^i, which is of the vector type, and the anisotropic stress tensor Σ_j^i which is a tensor.

The inflaton perturbations influence the evolution of the metric perturbations through Einstein equations, this means that the two sets are tightly connected.

2.1.3 Gauge invariance

While talking about perturbations, it is important to also mention the dependence on the gauge choice. In fact, spacetime coordinates $\mathbf{x}$ and τ are not uniquely defined in generic perturbed spacetimes, and the way we choose the slicing (time coordinate choice) and threading (space coordinate choice) can fundamentally change the definition of the perturbations. Given a tensor field X and a vector δX, a gauge transformation of the coordinates is by definition a Lie derivative

$$X \quad \rightarrow \quad \tilde{X} = X + \mathcal{L}_{\delta\mathbf{x}} X \tag{2.1.15}$$

that corresponds to a redefinition of spacetime coordinates of the form:

$$t \quad \rightarrow \quad t + \alpha \tag{2.1.16}$$

$$x^i \quad \rightarrow \quad x^i + \delta^{ij}\beta_j \ . \tag{2.1.17}$$

The perturbations generated by such transformations are not physical and need not be considered, because they can be simply removed through another coordinate transformation. We report here the infinitesimal changes of the relevant perturbations under the aforementioned gauge transformation:

1. Scalar metric perturbations:

$$\Phi \rightarrow \Phi - \dot{\alpha} \tag{2.1.18}$$
$$B \rightarrow B + a^{-1}\alpha - a\dot{\beta} \tag{2.1.19}$$
$$E \rightarrow E - \beta \tag{2.1.20}$$
$$\Psi \rightarrow \Psi + H\alpha \, . \tag{2.1.21}$$

2. Scalar matter perturbations:

$$\delta\rho \rightarrow \delta\rho - \dot{\bar{\rho}}\alpha \tag{2.1.22}$$
$$\delta p \rightarrow \delta p - \dot{\bar{p}}\alpha \tag{2.1.23}$$
$$\delta q \rightarrow \delta q + (\bar{\rho} + \bar{p})\alpha \, . \tag{2.1.24}$$

3. Tensor perturbations of both metric and matter are gauge-invariant, and such an invariance is a defining characteristic of these perturbations

To solve the ambiguity of the spacetime coordinates definition for scalar perturbations, it is convenient to work with gauge-invariant quantities that can be obtained by linear combinations of the previously illustrated gauge-dependent perturbations. This formulation of perturbation theory in a gauge-invariant framework was first proposed by Bardeen [17].

A convenient example of gauge-invariant perturbation, that we are going to use in the rest of this chapter, is the comoving curvature perturbation:

$$\mathcal{R} \equiv \Psi - \frac{H}{\bar{\rho} + \bar{p}}\delta q \; = \; \Psi + \frac{H}{\dot{\bar{\phi}}}\delta\phi \, . \tag{2.1.25}$$

The second relation comes from the fact that during inflation $T^0_i = \partial_i \delta q = -\dot{\bar{\phi}}\, \partial_i \delta\phi$. This perturbation is linked to the choice for the slicing and threading, called comoving gauge, associated to hypersurfaces with constant values of the inflaton ϕ:

$$\delta\phi = 0 \tag{2.1.26}$$
$$g_{ij} = a^2[(1 - 2\mathcal{R}\delta_{ij}) + h_{ij}] \tag{2.1.27}$$
$$\tag{2.1.28}$$

that is also equivalent to the choice:

$$\delta q = 0 \tag{2.1.29}$$

$$E = 0 \, . \tag{2.1.30}$$

In this gauge, $\mathcal{R}$ parametrizes the scalar degrees of freedom, and measures the spatial curvature, which is quantified by the Ricci tensor

$$R^{(3)} = \frac{4}{a^2}\nabla^2\mathcal{R} \, . \tag{2.1.31}$$

Other gauge-invariant quantities that are often used in literature are:

1. The constant-density-hypersurfaces curvature perturbation

$$\zeta \equiv -\Psi - \frac{H}{\dot{\bar{\rho}}}\delta\rho \, . \tag{2.1.32}$$

2. The inflaton perturbation on spatially flat slices

$$Q \equiv \delta\phi + \frac{\dot{\bar{\phi}}}{H}\Psi \, . \tag{2.1.33}$$

These quantities are all used in different contexts in the theory, according to which one is more appropriate in each case, but the final results on observable quantities are independent of the gauge choice.

The dynamics of all types of perturbations until now is described by the Einstein equations (2.1.2). Working at linear order in the perturbations introduced in (2.1.4) and (2.1.7), the resulting equations are:

1. Two constraint equations:

$$3H(\dot{\Psi} + H\Phi) + \frac{k^2}{a^2}\left[\Psi + H(a^2\dot{E} - aB)\right] = -4\pi G\delta\rho \tag{2.1.34}$$

$$\dot{\Psi} + H\Phi = -4\pi G\delta q \, . \tag{2.1.35}$$

2. Two evolution equations:

$$\ddot{\Psi} + 3H\dot{\Psi} + H\dot{\Phi} + (3H^2 + 2\dot{H})\Phi = 4\pi G\left(\delta p - \frac{2}{3}k^2\delta\Sigma\right) \tag{2.1.36}$$

$$(\partial_t + 3H)\left(\dot{E} - \frac{B}{a}\right) + \frac{\Psi - \Phi}{a^2} = 8\pi G\delta\Sigma \, . \tag{2.1.37}$$

3. The continuity equation (from conservation of energy-momentum tensor):

$$(\dot{\delta\rho}) + 3H(\delta\rho + \delta p) = \frac{k^2}{a^2}\delta q + (\bar{\rho} + \bar{p})\left[3\dot{\Psi} + k^2\left(\dot{E} + \frac{B}{a}\right)\right] . \tag{2.1.38}$$

4. The Euler equation (also from the conservation of energy-momentum tensor):

$$(\dot{\delta q}) + 3H\delta q = -\delta p + \frac{2}{3}k^2\delta\Sigma - (\bar{\rho} + \bar{p})\Phi . \tag{2.1.39}$$

By combining these equations and writing them in terms of the comoving curvature perturbation, we obtain the Einstein equations in the comoving gauge:

$$\frac{k^2}{a^2}[-\mathcal{R} - aHB] = -4\pi G\delta\rho \tag{2.1.40}$$

$$-\ddot{\mathcal{R}} + H\dot{\Phi} + 2\dot{H}\Phi = 4\pi G\left(\delta p - \frac{2}{3}k^2\delta\Sigma\right) \tag{2.1.41}$$

$$(\partial_t + 3H)\frac{B}{a} + \frac{\mathcal{R} + \Phi}{a^2} = -8\pi G\delta\Sigma . \tag{2.1.42}$$

The continuity and Euler equations are instead:

$$(\dot{\delta\rho}) + 3H(\delta\rho + \delta p) = (\bar{\rho} + \bar{p})\left[-3\dot{\mathcal{R}} + k^2\frac{B}{a}\right] \tag{2.1.43}$$

$$-\delta p + \frac{2}{3}k^2\delta\Sigma - (\bar{\rho} + \bar{p})\Phi = 0 . \tag{2.1.44}$$

2.1.4 Observable quantities

From the gauge-invariant variables, we can derive quantities that can be compared with experimental observations. In particular, we are interested in the amplitude of scalar and tensor perturbations. To define the amplitude of a general variable X, first we start by defining the power spectrum of the Fourier components of such variable, that can be expanded as an operator in the following way:

$$X \to \hat{X} = \int \frac{\mathrm{d}\mathbf{k}^3}{(2\pi)^3}\left[X_k(\tau)\hat{a}_{\mathbf{k}}e^{i\mathbf{k}\cdot\mathbf{x}} + X_k^*(\tau)\hat{a}_{\mathbf{k}}^\dagger e^{-i\mathbf{k}\cdot\mathbf{x}}\right] \tag{2.1.45}$$

Taking the expectation value of the modes X_k:

$$\langle X_k X_{k'}\rangle = (2\pi)^3\delta(k + k')|X_k|^2 \tag{2.1.46}$$

We call the power spectrum associated to X the quantity:

$$\mathcal{P}_X(k) \equiv \frac{k^3}{2\pi^2}|X_k|^2 \ . \tag{2.1.47}$$

We can use this formalism to define the power spectra of scalar fluctuations:

$$\mathcal{P}_s(k) = \frac{k^3}{2\pi^2}|\mathcal{R}_k|^2 \tag{2.1.48}$$

and of tensor fluctuations:

$$\mathcal{P}_t(k) \equiv \frac{k^3}{\pi^2}|h_k|^2 \ . \tag{2.1.49}$$

The power spectrum (2.1.49) is the sum of the spectra for the two polarization modes of h_{ij}:

$$\mathcal{P}_t(k) = \mathcal{P}_{h^+}(k) + \mathcal{P}_{h^\times}(k) \ . \tag{2.1.50}$$

This motivates the extra factor of 2 present in (2.1.49), we will see this in greater detail in a following section.

Having derived the two power spectra, we can now define the two main observables that are used to evaluate inflation models in the literature. These are the scalar spectral index:

$$n_s - 1 \equiv \frac{d\ln \mathcal{P}_s(k)}{d\ln k} \tag{2.1.51}$$

and the tensor-to-scalar ratio:

$$r \equiv \frac{\mathcal{P}_t(k)}{\mathcal{P}_s(k)} \ . \tag{2.1.52}$$

2.1.5 Sub-horizon and super-horizon regimes

For the evolution of perturbation Fourier modes, it will be later important to distinguish between two regimes, called sub-horizon and super-horizon regimes. The sub-horizon regime is when $k \gg aH$, this means that the characteristic length scale of the perturbations is significantly smaller than the comoving Hubble scale; viceversa, the super-horizon regime corresponds to $k \ll aH$. We call "horizon crossing" the moment in cosmic time when $k = aH$, so when the mode enters or exits the super-horizon regime. This event is important in the spectrum calculation, because in the standard slow-roll regime, which is the starting point for treating inflationary perturbations, the spectrum approaches a constant value with respect to cosmic time after horizon crossing. One usually says that the mode *freezes* in super-horizon regime. When this transition happens, the quantum fluctuations can be seen as classical, because the number of particles quanta related to each quantum mode k is much larger than unity. In particular, for quantum modes

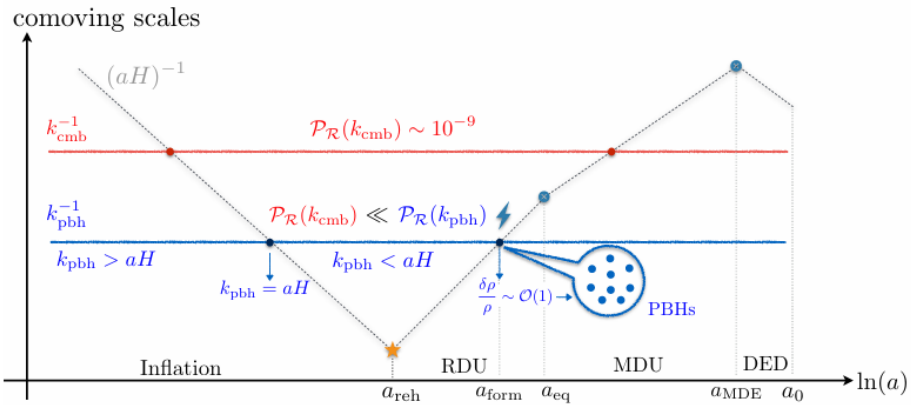

Figure 2.1: In this graph from [13], the comoving Hubble radius evolution is illustrated, along with the length scales of scalar perturbations, represented by k^{-1}, as function of the number of e-folds. In particular, we have two important cases, which are the CMB scale, which exits at the beginning of inflation, and the PBH scale, which exits many e-folds later. Starting from reheating, the comoving Hubble radius starts to grow, and eventually every mode re-enters the horizon, causing the formation of large-scale structures on a wide range of scales.

related to scalar fluctuations, the result is

$$n_k \sim \left(\frac{k}{aH}\right)^{-4} \quad \Longrightarrow \quad n_k \gg 1 \,. \tag{2.1.53}$$

2.2 Mukhanov-Sasaki equation and power spectrum

In this section, we are going to examine the dynamics of scalar curvature perturbations, starting from the action associated with the comoving curvature $\mathcal{R}$. We are going to look first at the dynamics of only the scalar perturbations, as this is the simpler case to treat, and then we shall briefly discuss the case of tensor perturbations, where the procedure is analogous to the scalar case for each of the two polarization directions. Also, to stick to a simpler case, we are going to consider the inflaton as minimally coupled to gravity.

2.2.1 Scalar perturbations spectrum

In the presence of a (quasi) de Sitter background, as it is during inflation, the scalar perturbations dynamics is described by the second-order action :

$$\mathcal{S}_{\mathcal{R}}^{(2)} = \frac{1}{2}\int d^4x\, a^3 \frac{\dot{\phi}^2}{H^2}\left[\dot{\mathcal{R}}^2 - a^{-2}(\partial_i \mathcal{R})^2\right] . \tag{2.2.1}$$

This action is obtained starting from the inflaton action (1.7.1) and inserting the perturbed quantities, keeping terms up to second order. This process is shown in appendix A, following the method used by Maldacena in [18].

On varying the action (2.2.1) we can get the equation that describes the evolution of the comoving curvature perturbation scalar through conformal time, but we are interested in a scale-dependent analysis of the perturbations, so we can shift to Fourier space in order to obtain the evolution equation of the modes $\mathcal{R}_k(\tau)$, each mode having wavenumber k:

$$\ddot{\mathcal{R}}_k + 2\frac{\dot{z}}{z}\dot{\mathcal{R}}_k + k^2\mathcal{R}_k = 0 \tag{2.2.2}$$

where the dot denotes the derivative with respect to conformal time, and the quantity $z(\tau)$ is called the pump field and is defined as:

$$z \equiv \frac{a\dot{\phi}}{H} . \tag{2.2.3}$$

The pump field dynamics is extremely important for the amplification process, because it represents the influence of the background dynamics on the perturbations. In general, the pump field is a model-dependent function of the slow-roll parameters ε_i.

Another compact form of Eq. (2.2.2) is:

$$\ddot{v_k} + \left(k^2 - \frac{\ddot{z}}{z}\right) v_k = 0 . \tag{2.2.4}$$

In this form, we used the function $v_k = z\mathcal{R}_k$.

To calculate the power spectrum, we have to start from the quantum origin of cosmological perturbations, so we have to quantize the v_k's. We start by promoting v_k to operators:

$$\hat{v}_k = v_k(\tau)\hat{a}_k + v_k^*(\tau)\hat{a}_k^\dagger \tag{2.2.5}$$

where, as in usual quantization processes, the annihilation-creation operators $\hat{a}_k$ and $\hat{a}_k^\dagger$

satisfy the commutation relations:

$$[\hat{a}_k, \hat{a}^\dagger_{k'}] = (2\pi)^3 \delta(k - k') \,. \tag{2.2.6}$$

To unambiguously define this Fock space, it is necessary to choose an additional initial condition that identifies the vacuum. Indeed, this choice is not unique, as our spacetime is curved and time-dependent. The standard choice is to impose a condition on the vacuum in the far past at $\tau \to -\infty$, so that it coincides with the Minkowski vacuum. The modes will have the following expression:

$$v_k|_{\tau\to-\infty} = \frac{e^{-ik\tau}}{\sqrt{2k}} \,. \tag{2.2.7}$$

This ansatz for the vacuum is called the Bunch-Davies vacuum [19]. Starting from the Bunch-Davies vacuum $|0\rangle$, the "particle states" are defined by applying the creation operators. This is how the perturbations are generated in the Early Universe.

In order to find the expression for the power spectrum, we have to calculate the evolution of the modes functions v_k. In the case of slow-roll inflation, this is a relatively easy task, as $\mathcal{R}_k$ becomes constant when the corresponding mode k crosses the horizon (when $k \approx aH$). The amplitude of the power spectrum at horizon crossing is a crucial quantity to compute, because the power spectrum reaches a constant value at the moment of horizon crossing and then stops evolving, until it re-enters the horizon at a later time.

In a regime different from the slow roll, $\mathcal{R}_k$ may evolve outside of the horizon. In this case, the evolution should always be calculated, and a numerical analysis is often used. In this thesis we will be interested in the ultra-slow-roll regime. It can be shown that evaluating the power spectrum in ultra-slow-roll dynamics by using the same expression that is obtained for slow-roll dynamics [20, 21] is a fairly good approximation. However, for a precise estimate of the spectrum, numerical solutions are necessary in order to find the final power spectrum. Some techniques to compute the evolution of perturbations in an analytical way do exist. In appendix B we will go over a technique that can be useful to find a form of the evolution of the power spectrum, while actively including the transient non-slow-roll phase. In this section, we limit ourselves to deriving the power spectrum expression in slow-roll dynamics, following references [9] and [18] for calculations.

Assuming a minimal inflaton coupling, the pump field is described by the expression:

$$z = a\sqrt{\varepsilon_1} \tag{2.2.8}$$

where ε_1 is the order-1 term in the hierarchy (1.7.7). Considering this, and taking the

limit $\varepsilon_1 \to 0$, the equation (2.2.4) becomes:

$$\ddot{v_k} + \left(k^2 - \frac{2}{\tau^2}\right) v_k = 0 \tag{2.2.9}$$

where we have evaluated

$$\lim_{\varepsilon_1 \to 0} \ddot{z}/z = 2/\tau^2 \ . \tag{2.2.10}$$

The general solution to Eq. (2.2.9) is:

$$v_k = -\frac{i}{\sqrt{2k^3}} H \left[C_1(1 + ik\tau)e^{-ik\tau} + C_2(1 - ik\tau)e^{ik\tau}\right] \ . \tag{2.2.11}$$

In order to determine the two arbitrary constants C_1 and C_2, we impose the Bunch-Davies vacuum condition and the normalization condition, thus obtaining $C_1 = 1$ and $C_2 = 0$:

$$v_k = \frac{e^{-ik\tau}}{\sqrt{2k}} \left(1 - \frac{i}{k\tau}\right) \ . \tag{2.2.12}$$

From this expression, it is immediate to calculate the power spectrum by its definition (2.1.46):

$$\langle \hat{v_k}, \hat{v_{k'}} \rangle = (2\pi)^3 \delta(k + k') |v_k|^2 = (2\pi)^3 \delta(k + k') \frac{H^2 a^2}{2k^3} (1 + k^2\tau^2) \ . \tag{2.2.13}$$

Now, remembering that the comoving curvature perturbation is $\mathcal{R}_k = \frac{v_k}{z}$, we can find the power spectrum of $\mathcal{R}_k$ by evaluating:

$$|\mathcal{R}_k|^2 = \left|\frac{v_k}{z}\right|^2 = \frac{1}{z^2} \frac{H^2 a^2}{2k^3} (1 + k^2\tau^2) = \frac{H^2}{\dot{\phi}^2} \frac{H^2}{2k^3} (1 + k^2\tau^2) \tag{2.2.14}$$

and, plugging this result in (2.1.48), we obtain the power spectrum:

$$\mathcal{P}_\mathcal{R}(k, \tau) = \frac{k^3}{2\pi^2} |\mathcal{R}_k|^2 = \frac{H^4}{4\pi^2 \dot{\phi}^2} (1 + k^2\tau^2) \ . \tag{2.2.15}$$

At superhorizon scales, from the defining condition $k/aH \ll 1$, we have that $k^2\tau^2 \ll 1$, because of the relation between conformal time and the scale factor:

$$\tau = \int \frac{dt}{a(t)} = \int \frac{dt}{e^{Ht}} = -\frac{1}{H} e^{-Ht} = -\frac{1}{aH} \quad \Longrightarrow \quad k^2\tau^2 = \frac{k^2}{(aH)^2} \ll 1 \ . \tag{2.2.16}$$

We obtain that, when the perturbation crosses the horizon, the term $k^2\tau^2$ in (2.2.15)

rapidly decreases, hence the power spectrum becomes constant and takes the value:

$$\mathcal{P}_{\mathcal{R}}(k) = \frac{H^4}{4\pi^2\dot{\phi}^2} \,. \tag{2.2.17}$$

2.2.2 Tensor perturbations spectrum

Although we will not directly work with tensor perturbations in the next chapters, it is important to study their original dynamics. In fact, the tensor perturbations spectrum expression is present in the definition of the tensor-to-scalar ratio r, which is an important parameter to be confronted with observations, that we will use later in this analysis. One can also define, in analogy with (2.1.51), a tensor spectral index n_t, which measures the deviation from scale-invariance of the tensor power spectrum, and use it as a measurable observable.

By expanding the perturbed Einstein-Hilbert action up to second order in h_{ij}, one obtains

$$S_h^{(2)} = \frac{M_P^2}{8} \int d^4x\, a^2 \left[(\dot{h}_{ij})^2 - (\partial_k h_{ij})^2\right] . \tag{2.2.18}$$

Since this type of perturbation is a massless scalar field, the idea to derive the spectrum is to expand the tensor perturbation in Fourier modes and sum over the two polarizations:

$$h_{ij} = \int \frac{d^3\mathbf{k}}{(2\pi)^3} \Sigma_s \epsilon_{ij}^s(k)\, h_k^s(\tau)\, e^{i\mathbf{k}\cdot\mathbf{x}} \tag{2.2.19}$$

where the tensorial index s can have two "values", $s = +, \times$, that represent the two types of polarization.

For each value of s, we define the field

$$v_k^s \equiv \frac{a}{2} M_P\, h_k^s \tag{2.2.20}$$

and by substituting in (2.2.18), the second-order action becomes

$$S_{(2)} = \sum_s \frac{1}{2} \int d\tau d^3k \left[(\dot{v}_k^s)^2 - \left(k^2 - \frac{\ddot{a}}{a}\right)(v_k^s)^2\right] . \tag{2.2.21}$$

Now we observe that this action leads to two equations of motion, one for each helicity, that are identical to (2.2.4). Each polarization of the gravitational wave behaves as a renormalized massless scalar field in de Sitter space, $h_{\mathbf{k}}^s = 2\psi_{\mathbf{k}}^s/M_P$, for which the power spectrum is proportional to (2.2.17), this means that the power spectrum for each mode

h_k^s is

$$\mathcal{P}_h^{(s)}(k) = \frac{H^2 a^2}{2k^3} \frac{4}{M_P^2 a^2} \frac{k^3}{2\pi^2} = \frac{H^2}{\pi^2 M_P^2} \,. \tag{2.2.22}$$

To get the total power spectrum of tensor perturbations we can simply sum the two spectra, obtaining the following result:

$$\mathcal{P}_h(k) = 2\,\mathcal{P}_h^{(s)}(k) = \frac{2H^2}{\pi^2 M_P^2} \,. \tag{2.2.23}$$

We can then observe that the tensor perturbations spectrum and the scalar perturbations spectrum satisfy the following relation:

$$\mathcal{P}_h = \frac{8\dot{\phi}^2}{M_P^2\, H^2} \mathcal{P}_s \,. \tag{2.2.24}$$

2.3 Amplification mechanisms

After the introduction on the dynamics of inflationary perturbations and the main related observables, in this section we will discuss, in a model-independent way, the mechanisms that can produce amplifications in the spectrum of scalar perturbations.

One way to produce amplifications is to design models in which the spectrum is heavily scale-dependent at horizon crossing. The idea would be that slow-roll parameters change considerably in a short time interval during inflation, contributing in a non-trivial way to the Mukhanov-Sasaki equation solution. In this case, the late-time power spectrum can be written in the following way:

$$\mathcal{P}_\mathcal{R}(k) = \frac{H^2}{8\pi^2 \varepsilon_1} (1 + \Theta) \tag{2.3.1}$$

where Θ is the non-trivial contribution.

Another possibility is to construct a scenario in which the spectrum becomes scale-dependent after horizon crossing. To explore this possibility, and keeping the discussion model-independent, we can look at a general solution of Eq. (2.2.2), obtained by using a gradient expansion approach:

$$u_k(\tau) = u_k^{(0)} \left[1 + \frac{\dot{u}_k^{(0)}}{u_k^{(0)}} \int_{\tau_0}^{\tau} \frac{d\tau'}{\tilde{z}^2(\tau')} - k^2 \int_{\tau_0}^{\tau} \frac{d\tau'}{\tilde{z}^2(\tau')} \int_{\tau_0}^{\tau} d\tau'' z^2(\tau'') \frac{u_k(\tau'')}{u_k^{(0)}} \right] \,. \tag{2.3.2}$$

To produce this expression, we can start from the constant solution $u_k^{(0)}$, which is the limit for small k/aH, then we include momentum-dependent corrections that solve (2.2.2)

order by order expanding around $k/aH \ll 1$. In slow-roll regime, after horizon crossing the pump field rapidly increases, and (2.3.2) reduces to the constant mode $u_k^{(0)}$, that produces a scale-invariant spectrum. Alternatively, if the pump field decreases after horizon crossing, the terms contained in the integrals grow instead of decaying. In terms of the gradient of the pump field, this condition can be written as:

$$\frac{z'}{z} = aH\left[1 + \frac{\varepsilon_2}{2}\right] < 0 \tag{2.3.3}$$

where $\varepsilon_2 = \frac{dln\varepsilon_1}{dN}$ is the second slow-roll parameter of the Hubble flow function hierarchy. Since the quantity aH stays positive during inflation, this is equivalent to saying that the slow-roll parameter ε_2 becomes negative and $\mathcal{O}(1)$ in this transient period. This can only happen in regimes different from slow-roll.

To understand the situation from a dynamical point of view, we can also look at the expression (2.2.17) for the amplitude of scalar perturbations in super-horizon regime that was derived in the previous section, and we report it here too:

$$\mathcal{P}_{\mathcal{R}}(k) = \frac{H^4}{4\pi^2\dot{\phi}^2}\,. \tag{2.3.4}$$

Starting from this expression in slow-roll regime, it is clear that, in order to increment the spectrum at certain scales, either H has to get bigger, or the gradient of the squared inflaton $\dot{\phi}^2$ has to become smaller. Since during inflation the Hubble parameter H is (almost) constant, looking at the denominator we see that the inflaton field has to further decelerate in order to produce an amplified spectrum.

2.4 Features of PBH-producing inflation models

In this section, we anticipate the general features of an inflationary model that leads to PBH production by spectrum enhancement.

2.4.1 Potential

To start, we can expect at least three different phases during inflation:

1. The initial slow-roll phase, during which the perturbations that are linked to CMB inhomogeneities exit the horizon, around the pivot scale $k_{cmb} = 0.05$ Mpc^{-1} ($N \approx 0$). These perturbations are often used, in model building, in order to tune free model parameters.

2. A second, intermediate phase in which the slow-roll regime is violated, and the

second slow-roll parameter becomes negative and $\mathcal{O}(1)$. As a result, during this phase the first slow-roll parameter also decays exponentially.

3. A third phase, which is again characterized by slow-roll regime, that leads to inflation end, and then reheating. Inflation ends when the parameter ε_1 becomes $\mathcal{O}(1)$.

In principle, there could be multiple sequences of non-slow-roll phases followed by slow-roll. This would add structure to the spectrum, and would need a thorough probing of the involved scales.

2.4.2 Power spectrum

To illustrate the features of the power spectrum during amplification, we can define, as in ref. [22], the following quantity:

$$\Pi_k(\tau) \equiv \frac{\mathcal{P}_{\mathcal{R}}(\tau)}{\mathcal{P}_{\mathcal{R}_{k\to 0}}(\tau)} \,. \tag{2.4.1}$$

This is the ratio between the power spectrum and its limit at large scales, and can be expressed analytically as a function of the conformal time:

$$\begin{aligned}\Pi_k(\tau) &= 1 + \tau^2 k^2 + \\ &+ \frac{\alpha^4}{4}\left[(k\Delta\tau)^2\left(\alpha - \frac{4\tau}{\Delta\tau}\right) - k\Delta\tau\left(\alpha - \frac{2\tau}{\Delta\tau}\right)\sin(2k\Delta\tau) + (\alpha-4)\sin^2(k\Delta\tau)\right] \,.\end{aligned} \tag{2.4.2}$$

This representation is characterized by the interval $\Delta\tau$, that is the interval of the non-attractor phase, the length scale k and the parameter α, that controls the growth of the spectrum (it represents the influence of non-slow-roll phases on the spectrum). For $k \to 0$ this function goes to 1. By tuning the parameters, this expression can parametrize the characteristic spectral curve of a general model, so by using it we keep the discussion model-independent.

It is useful to rewrite (2.4.2) as function of the parameter $\eta \equiv k\tau$:

$$\begin{aligned}\Pi_k(\tau) &= 1 + \eta^2 + \\ &+ \frac{\alpha^4}{4}\left[\left(\eta\frac{\Delta\tau}{\tau}\right)^2\left(\alpha - \frac{4\tau}{\Delta\tau}\right) - \eta\frac{\Delta\tau}{\tau}\left(\alpha - \frac{2\tau}{\Delta\tau}\right)\sin\left(2\eta\frac{\Delta\tau}{\tau}\right) + (\alpha-4)\sin^2\left(\eta\frac{\Delta\tau}{\tau}\right)\right] \,.\end{aligned} \tag{2.4.3}$$

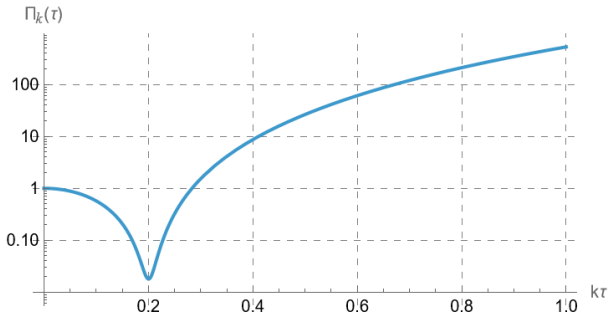

Figure 2.2: In this graph we plot an approximate profile of the perturbation spectrum in a model that admits amplification. The parameters used in this graph are $\alpha = 200$ and $\Delta\tau/\tau = 0.5$.

We can expand this expression for $k\tau \ll 1$ (super-horizon regime) to obtain:

$$\Pi_k(\tau) = 1 - \eta^2 \left(\alpha \frac{\Delta\tau^2}{\tau^2} - 1 \right) + \mathcal{O}(\eta^4) \,. \tag{2.4.4}$$

Here we notice that, while for $k \to 0$ the expression goes to 1. As k gets larger the second term becomes more important in the expansion, causing the spectrum to decrease, until the term $\sim \eta^4$ becomes large enough to cause the spectrum to increase. These two phases are visible in the characteristic dip, which is present before the amplification in every enhanced spectrum. An example of such profile is shown in Fig. (2.2), with parameters $\alpha = 200$ and $\Delta\tau/\tau = 0.5$. If we Taylor-expand the periodic functions in (2.4.2), and consider larger values of k, we obtain that the highest order in k that contributes to the growth of the spectrum is k^4, this is because the higher-order term has a negative coefficient that causes the spectrum to decrease. We can then conclude that, independently of the model, the maximum achievable growth of the spectrum is $\sim k^4$, which corresponds to a scalar spectral index $n_s - 1 = 4$.

2.4.3 Ultra-slow-roll regime (USR)

The ultra-slow-roll regime was first studied by Kinney [23] and since then it has been the most prominent mechanism used in literature in order to obtain spectrum amplifications. Ultra-slow-roll inflation is realized when the potential's gradient is negligible, $V'(\phi) \simeq 0$, this happens when there is a flat plateau in $V(\phi)$. In this case, the inflaton field slows down, and the Klein-Gordon equation (1.7.4) will become:

$$\ddot{\phi} + 3H\dot{\phi} \simeq 0 \,. \tag{2.4.5}$$

In this situation, one of the slow-roll condition is violated because the slow-roll parameter ε_2 has a negative and relatively large value, due to its connection to the dynamics of parameter ε_1.

A generalization of the ultra-slow-roll regime was proposed in 2014 by Motohashi, Starobinsky and Yokoyama [24], and it is called constant-roll inflation. In this case, the requirement is that the inflaton field has constant roll, so:

$$\frac{\ddot{\phi}}{H\dot{\phi}} = \beta\,. \tag{2.4.6}$$

The ultra-slow-roll case is the specific case in which $\beta = 3$. From a dynamical point of view, this regime can be realized with a non-flat potential, that has the inflaton going up from a dip on a local maximum for a transient period, therefore the field velocity is not constrained to be small.

During this work, we are going to focus on the ultra-slow-roll regime, so we will consider $\beta = 3$. We can rewrite Eq. (2.4.6) in terms of the slow-roll parameters, obtaining this form:

$$2\varepsilon_1^2 - \varepsilon_1\varepsilon_2 + 6\varepsilon_1 = 0 \tag{2.4.7}$$

This equation has one exact de Sitter solution where $\varepsilon_1 = 0$, and one solution that is approaching the de Sitter solution:

$$\varepsilon_1 \to 0 \quad , \quad \varepsilon_2 \to -6 \tag{2.4.8}$$

This second solution is a consequence of the presence of the de Sitter solution, because it's the case in which the system is approaching the de Sitter attractor.

In terms of the field flow function hierarchy, Eq. (2.4.6) can be written as:

$$\delta_1(\delta_2 + \delta_1 - \varepsilon_1) - 3\delta_1 = 0 \tag{2.4.9}$$

Assuming that $\varepsilon_1 \to 0$, this system has one exact solution where $\delta_1 = 0$, and one solution where it's approaching the latter:

$$\delta_1 \to 0 \quad , \quad \delta_2 \to 3 \tag{2.4.10}$$

Chapter 3

Primordial black holes formation

After going over the theory of inflationary perturbations in the previous chapter, we will explain the physics of primordial black holes (PBHs) and study extensively how the theory of PBHs is related to the spectrum amplification of inflation.

In the last decades, the theory of inflation has been thoroughly tested and supported by observations of the CMB inhomogeneities and large scale structures. However, these probes cover only a small portion of the cosmological scales that characterize perturbations, namely the largest ones (the ones that exit the horizon at earlier times, $10^{-4} \lesssim k\,[\mathrm{Mpc}^{-1}] \lesssim 10^{-1}$), so the observational data leaves out most of the inflation epoch.

However, in the recent years, a new possibility has attracted a lot of interest. Following the 2015 observation of gravitational waves, detected by the LIGO/VIRGO collaboration [25], it has been considered the possibility that the merging of primordial black holes originated these detected events. This possibility is very interesting because it would offer a way to probe inflationary dynamics at new scales. Moreover, PBHs are interesting dark matter candidates, because, given the experimental constraints, they satisfy the requirements to be dark matter without the need to introduce new beyond-standard-model physics in the picture.

In this chapter, we will first discuss the formation mechanism and key features of PBHs, then we will explain how these features are related to the amplification of the perturbation spectrum. We will conclude by discussing the current state of PBHs as dark matter candidates, commenting on the experimental limits on the abundance and the masses.

3.1 PBH formation and relevant variables

Primordial black holes could originate from the gravitational collapse of density perturbations in regions of the Early Universe where the density exceeds a critical value. Density perturbations are seeded from scalar perturbations, which, as we studied in chapter (2), are generated by quantum fluctuations of the inflaton field in the early stages of inflation. The evolution of scalar perturbations is characterized by three phases: first, they form inside the comoving horizon ($k \gg aH$), then they exit this horizon at $k \approx aH$, to then re-enter again after the end of inflation, when the comoving horizon starts to increase again. At typical PBH scales, the perturbations re-enter during the radiation-dominated era, which occurs after reheating but before the matter-dominated era. At that time, the scalar inflaton perturbations are imprinted in the density perturbations, defined as:

$$\delta \equiv \frac{\delta\rho}{\rho} \sim \mathcal{P}_{\mathcal{R}}(k)^{1/2} \, . \tag{3.1.1}$$

When the density fraction δ exceeds a certain threshold, that we will call δ_c, the matter collapses and forms a black hole. In the next sections we are going to see how this collapse threshold is estimated, and we introduce other quantities that will be relevant for connecting experimental results with theory. The main references for these sections are the reviews [13, 26].

3.1.1 Threshold of collapse

The first estimate for the collapse threshold was made by Carr and Hawking in 1974 [3], and is based on a Jeans-type instability argument in newtonian gravity. The overdensity region collapses if δ is larger than the square of the sound speed of density perturbations, so

$$\delta \gtrsim c_s^2 \, . \tag{3.1.2}$$

This condition means that the signal that carries the gravitational pull travels faster than the pressure waves that contrast it, so that gravity dominates over pressure, allowing the collapse. Since the sound speed of perturbations is $c_s^2 = \omega$ and during the radiation domination era the equation of state is $\omega = 1/3$, the threshold estimate is

$$\delta_c \simeq 0.4 \, . \tag{3.1.3}$$

Throughout the years, more refined estimates were made and it became clear that the threshold depends on the shape of the curvature perturbation, as well as on the equation of state of the fluid, since the larger is ω, the larger the pressure gradient is, and the

higher is the threshold.

Another important criterion for the threshold was formulated in 1999 [27], when it was suggested that the PBH formation may occur at the peak of the compaction function, which is a function that represents the average mass excess in a given volume. In [28] simulations have been performed using many different perturbations profiles, leading to a range of critical overdensities in the radiation-dominated Universe:

$$\delta_c \approx 0.4 - 2/3 \; . \tag{3.1.4}$$

In [29, 30] it was found that, although δ_c is a profile-dependent quantity, an approximately universal estimate is $\delta_c \sim 0.4$. This value only slightly depends on the nature of the cosmic fluid and on the curvature around the peak of the compaction function.

3.1.2 Mass

An analytical estimate to obtain PBH masses was developed by Carr [4]:

$$M_{pbh} = \gamma M_H^{(eq)} \left(\frac{M_H^{(f)}}{M_H^{(eq)}} \right) = \left(\frac{a_f}{a_{eq}} \right)^2 \gamma M_H^{(eq)} \; . \tag{3.1.5}$$

In this formula, M_H is the time-dependent mass contained in the Hubble horizon $1/H(t)$:

$$M_H \equiv \frac{4\pi\rho(t)}{3H(t)^3} \tag{3.1.6}$$

and the subscripts f and eq respectively denote quantities evaluated at the time of PBH formation and at matter-radiation equality time. The second equality is obtained because in the radiation-dominated Universe we have $H^2 \sim \rho \sim a^{-4}$. The mass $M_H^{(eq)}$ is known and its value is $\sim 2.8 \cdot 10^{17} M_\odot$.

It is useful to relate the PBH mass at formation to the perturbations modes leaving the horizon during inflation. Rewriting (3.1.5) as function of ρ and H, knowing that the energy density scales as $\rho \propto g_*(T)T^4$ during radiation domination and considering entropy conservation for which $g_s(T)T^3a^3$ is a constant, we obtain:

$$M_{pbh}(k_{pbh}) = \left(\frac{g_*(T_f)}{g_*(T_{eq})} \right)^{1/2} \left(\frac{g_s(T_{eq})}{g_s(T_f)} \right)^{2/3} \left(\frac{k_{eq}}{k_{pbh}} \right)^2 \gamma M_H^{(eq)} \tag{3.1.7}$$

where $g_*(T)$ and $g_S(T)$ are the effective numbers of degrees of freedom considered respectively in the energy density and in the entropy.

Now, we can look at recent Planck results [31], that give us $k_{eq} \simeq 0.0104 Mpc^{-1}$, and

assuming that $g_*(T_{eq}) \simeq 3.38$ and that $g_*(T) = g_s(T)$ we obtain:

$$M_{pbh}(k_{pbh}) \simeq \left(\frac{\gamma}{0.2}\right)\left(\frac{g_*(T_f)}{106.75}\right)^{-1/6}\left(\frac{k_{pbh}}{3.2\cdot 10^5 Mpc^{-1}}\right)^{-2} 30M_\odot \ . \tag{3.1.8}$$

This equation tells us that, for a PBH mass $M_{pbh} \simeq 30M_\odot$, which could be observed by LIGO, the scale k_{pbh}^{-1} is smaller than k_{cmb}^{-1}. This direct relation ((3.1.8)) between k and M_{pbh} gives us an estimate of the inflationary perturbations modes eligible for PBH formation, considering different mass ranges from observations.

We can also derive a relation between the mass at formation and the number of e-folds at horizon exit, starting from (3.1.7) and considering that $k_{pbh}/k_{cmb} = (aH)_{pbh}/(aH)_{cmb}$ at horizon exit time. Then, we can relate H and a at the two exit times, considering the parameter ε_1 to be nearly constant:

$$H_{pbh} = H_{cmb}\, e^{-\varepsilon_1(N_{pbh}-N_{cmb})} \quad , \quad a_{pbh} = a_{cmb}\, e^{(N_{pbh}-N_{cmb})} \ . \tag{3.1.9}$$

Using these two relations in (3.1.7) and considering $k_{cmb} = 0.002 Mpc^{-1}$, we find the following equation:

$$M_{pbh}(N_{pbh}) \approx 7.7\cdot 10^{17} M_\odot e^{-2(N_{pbh}-N_{cmb})(1-\varepsilon_1)}\left(\frac{\gamma}{0.2}\right)\left(\frac{g_*(T_f)}{106.75}\right)^{-1/6} \ . \tag{3.1.10}$$

3.1.3 Abundance

The abundance of PBHs is their fraction of energy density compared to the total energy density in the Universe, and we refer to such fraction as Ω_{pbh}. The quantity Ω is defined for each type of energy content present in the Universe. One is typically interested in these ratios today:

$$\Omega_{i,0} \equiv \frac{\rho_{i,0}}{\rho_{c,0}} \tag{3.1.11}$$

where $\rho_{c,0}$ is the critical density for having a flat Universe at the present time ($\rho_{c,0} = 3H_0^2 M_{pl}^2$). In particular, for PBHs we are interested in the following ratio:

$$f_{pbh} \equiv \frac{\Omega_{pbh,0}}{\Omega_{dm,0}} \ . \tag{3.1.12}$$

This represents the abundance of PBHs in dark matter, for which we know the energy density in our Universe, which, according to the most recent data, is [31]

$$\Omega_{dm,0}h^2 = 0.120 \pm 0.001 \tag{3.1.13}$$

where $h = [0.6736 \pm 0.0054] \cdot 100\,\mathrm{km\ s^{-1}Mpc^{-1}}$ is a measure of the Hubble rate H_0. The quantity (3.1.12) can be linked to the density fraction of PBHs at the moment of their formation:

$$\beta \equiv \frac{\rho_{pbh,f}}{\rho_f} \tag{3.1.14}$$

where the subscript f denotes that the quantity is evaluated at the time of formation. Considering that after formation $\rho_{pbh} \propto a^3$:

$$\frac{\rho_{pbh,f}}{\rho_f} = \frac{\rho_{pbh,f}}{\rho_{pbh,0}} \frac{\rho_{crit,0}}{\rho_f} \Omega_{dm,0} f_{pbh} = \frac{\rho_{pbh.f}}{\rho_{pbh,0}} \frac{\rho_{crit,0}}{\rho_{eq}} \frac{\rho_{eq}}{\rho_f} \Omega_{dm,0} f_{pbh} \simeq \frac{1}{2} \frac{a_f}{a_{eq}} \Omega_{m,0}^{-1} \Omega_{dm,0} f_{pbh} \tag{3.1.15}$$

where $\Omega_{m,0}$ is the current matter density in the Universe, and the scale factor today is normalized $a_0 = 1$. This result can be related to the PBH mass by re-expressing the factor a_f/a_{eq} as follows:

$$\frac{a_f}{a_{eq}} = \frac{T_{eq}}{T_f} \left(\frac{g_s(T_{eq})}{g_s(T_f)} \right)^{1/3} \simeq 3.17 \cdot 10^{-9} \left(\frac{\gamma}{0.2} \right)^{-1/2} \left(\frac{g_*(T_f)}{106.75} \right)^{-1/12} \left(\frac{M_{pbh}^f}{M_\odot} \right)^{1/2} \tag{3.1.16}$$

where in the last equality we used Eq. (3.1.7) to make explicit the dependence on M_{pbh}^f. The resulting relation is:

$$\beta \simeq 1.33 \times 10^{-9} \left(\frac{\gamma}{0.2} \right)^{-1/2} \left(\frac{g_*(T_f)}{106.75} \right)^{-1/12} \left(\frac{M_{pbh,f}}{M_\odot} \right)^{1/2} f_{pbh}\ . \tag{3.1.17}$$

This formula allows us to evaluate the fraction of PBHs at formation for a range of possible masses and f_{pbh} values.

Another way to interpret β is the fraction of regions in the Universe whose density is over the threshold:

$$\beta \equiv \int_{\delta_c}^{\infty} P(\delta) d\delta\ . \tag{3.1.18}$$

$P(\delta)$ is the probability distribution function that describes how likely it is for a given region to have an overdensity δ, and we consider cases in which the overdensity is above the critical value. This definition is based on the Press-Schechter model of gravitational collapse [32], which is widely used in the study of large-scale structure formation. In this model, masses are considered part of a "gas" and their interactions are modeled as nonlinear N-body interactions.

Assuming that the probability distribution function can be modeled as a gaussian distribution with mean value $\mu = 0$, integrating (3.1.18) we find:

$$\beta \simeq \frac{\sigma}{\sqrt{2\pi}\delta_c} \exp\left(-\frac{\delta_c^2}{2\sigma^2} \right)\ . \tag{3.1.19}$$

Comparing with Eq. (3.1.17), we can find an estimate for the variance; for example, to produce a population of PBHs having $M \sim M_\odot$ and $f_{pbh} = 10^{-3}$ we need a ratio $\delta_c/\sigma \simeq 7$. Using the data on δ_c, we can estimate σ for several values of PBH masses, or directly as a function of the PBH abundance.

3.2 Conditions on the amplification

Before commenting on the results of the latest experiments, we will see how PBH properties discussed in the previous section can be related to the theory of cosmological perturbations, so that we will be able to link observations with theoretical models.

We can start by taking the fractional overdensity δ and Taylor expanding at leading order in a gradient expansion, working in Fourier space:

$$\delta(x,t) \simeq \frac{2(1+\omega)\nabla^2\mathcal{R}}{(5+3\omega)(aH)^2} \quad \Longrightarrow \quad \delta_k \simeq -\frac{4}{9}\left(\frac{k}{aH}\right)^2 \mathcal{R}_k \tag{3.2.1}$$

where ω is $1/3$ in the radiation dominated epoch. Given this relation between Fourier modes of the two functions δ and $\mathcal{R}$, and given the definition of power spectrum (2.1.46), we find the following relation between the spectra of δ and $\mathcal{R}$:

$$\mathcal{P}_\delta(k) \simeq \frac{16}{81}\left(\frac{k}{aH}\right)^4 \mathcal{P}_\mathcal{R}(k)\ . \tag{3.2.2}$$

Now, by looking at the variance of (3.1.19), it is possible to relate this latter parameter directly with $\mathcal{P}_\mathcal{R}$. The variance can be written, as a function of the power spectrum, in the following way [33]:

$$\sigma^2(R) = \int_0^\infty d\ln q\, \mathcal{W}^2(q,R)\, \mathcal{P}_\circ(q) \tag{3.2.3}$$

where $\mathcal{W}(q,R)$ is the Fourier transform of a real space window function that is used to smooth the overdensity on a scale $R \approx k^{-1} \approx (aH)^{-1}$. If the power spectrum $\mathcal{P}_\circ$ is peaked around the wave number k_{pbh}, the integral above can be approximated to $\sigma^2 \sim \mathcal{P}_\circ(k_{pbh})$, and considering also the result (3.2.2), the relation (3.2.3) becomes:

$$\sigma^2(R) \simeq \frac{16}{81}\mathcal{P}_\mathcal{R}(k_{pbh})\ . \tag{3.2.4}$$

The final relation between the variance σ and the perturbation power spectrum can be written as:

$$\mathcal{P}_\mathcal{R}(k_{pbh}) \sim 5\sigma^2\ . \tag{3.2.5}$$

According to Eq. (3.1.19), the dependence of the abundance β on the variance σ is

exponential, therefore a small change in the latter can cause a large variation in the former. This means that we can establish a criterion for $\mathcal{P}_\mathcal{R}(k)$ that covers a relatively large interval of values for β. For the range $10^{-3} \leq f_{pbh} \leq 1$, we find:

$$\mathcal{P}_\mathcal{R}(k_{pbh}) \sim 5\sigma^2 \sim 10^{-2} \, . \tag{3.2.6}$$

This result covers the mass range for PBHs $10^{-12} M_\odot \leq M^f_{pbh} \leq M_\odot$, but the estimate doesn't change much for even smaller PBH masses. Indeed, we could consider the smallest value of PBH mass that is allowed by current experiments, which is $M_{pbh} \simeq 10^{-18} M_\odot$, and corresponds to $f_{pbh} \leq 10^{-9}$. Considering the results in the previous section, this would correspond to the constraint $\mathcal{P}_\mathcal{R}(k_{pbh}) \leq 6 \times 10^{-3}$, which is included in the latter estimate.

We conclude by observing that, given that the typical order of magnitude of the spectrum at CMB scales is $\mathcal{P}_\mathcal{R}(k_{cmb}) \sim 10^{-9}$, the amplification that we need is about 7 orders

$$\Delta\mathcal{P}_\mathcal{R} \equiv \frac{\mathcal{P}_\mathcal{R}(k_{pbh})}{\mathcal{P}_\mathcal{R}(k_{cmb})} \sim 10^7 \, . \tag{3.2.7}$$

3.2.1 Case of non-gaussian overdensity distribution

In the former section, it was assumed that the probability distribution function of the overdensity was gaussian and, since they are proportional, also that of primordial curvature perturbations. In this section, we comment on the effects of the eventual non-gaussianity of the PDFs, which can have an important impact on the overall result. In particular, we comment on the representative case in which $\mathcal{R} = g^2 - \langle g^2 \rangle$, where g is a gaussian variable having mean 0 and variance $\langle g^2 \rangle$. The probability distribution function for $\mathcal{R}$ in this case is:

$$P(\mathcal{R}) = \frac{e^{-(\mathcal{R}+\langle g^2 \rangle)/2\langle g^2 \rangle}}{\sqrt{8\pi(\mathcal{R} + \langle g^2 \rangle)\langle g^2 \rangle}} \, . \tag{3.2.8}$$

The fraction of regions that can collapse into PBHs is then:

$$\beta = \int_{\mathcal{R}_{crit}}^{\infty} \mathrm{d}\mathcal{R} \, P(\mathcal{R}) \simeq \frac{1}{2} \mathrm{Erfc}\left(\sqrt{\frac{1}{2} + \frac{\mathcal{R}_{crit}}{\sqrt{2\mathcal{P}_\mathcal{R}}}} \right) \tag{3.2.9}$$

where the variance of $P(\mathcal{R})$ has been approximated to $\mathcal{P}_\mathcal{R}$ to include the curvature power spectrum. Combining this result with the expression (3.1.17) for the PBH abundance, we observe that a population of solar-mass PBHs having $f_{pbh} = 10^{-3}$ would require, in the case of non-gaussianity, an amplitude of the power spectrum $\mathcal{P}_\mathcal{R}(k_{pbh}) \sim 10^{-3}$. This result is valid for a large range of masses and values of the abundance. Compared to the result (3.2.6) in the previous section, the required amplification would be of about

6 orders of magnitude. This less stringent constraint allows for a more efficient PBH formation.

3.3 Primordial black holes as dark matter candidate

Primordial black holes within a certain mass interval satisfy all the necessary requirements to be good dark matter candidates. Indeed, they are cold, stable with respect to cosmological time scales, and, since they formed before nucleosynthesis, they are also non-baryonic, so they do not interact with other particles other than through gravity. A great advantage is also that PBHs are not new particles, so their origin would not require to modify or enlarge the Standard Model. However, there are many experimental limits to consider, that strongly constrain their mass and abundance ranges.

3.3.1 Constraints

In this first section, we will review the most recent experimental constraints on PBH abundance β, that is linked to PBH mass constraints through the relations presented in the previous sections. We will also discuss which mass ranges allow for PBHs to be viable dark matter candidates. We will mainly follow the review by Carr and Kuhnel [34].

Evaporation constraints

Considering Hawking radiation, a PBH of initial mass M will evaporate in a time scale $T \propto M^3$. This scale is less than the present age of the Universe if the mass is lower than $M_* \equiv 5 \times 10^{14}$ g, which is a lower bound for PBH masses, $M \gtrsim M_*$. Considering $M > 2M_*$, we can neglect the change in mass, and calculate a bound based on the observed spectrum of photons coming from each PBH. Calculating the instantaneous spectrum of primary photons, one finds at $E^{max} \propto M^{-1}$:

$$I^{max}(M) \propto f_{pbh}(M)\, M^{-2}\,. \tag{3.3.1}$$

Whereas the observed intensity is

$$I^{obs}(M(E)) \propto E^{-(1+\epsilon)} \tag{3.3.2}$$

with $0.1 < \epsilon < 0.4$. By requiring that $I^{max}(M) < I^{obs}(M)$ one obtains the following constraint [35]

$$f(M) < 2 \times 10^{-8} \left(\frac{M}{M_*}\right)^{3+\epsilon}\,. \tag{3.3.3}$$

Other notable bounds for other ranges of M come from positron data from Voyager 1 [36] constraining $f < 0.001$ for masses $M < 10^{16}$ g, from observations of $\gamma-$ray and radio emissions from the galactic centre and from the observed reionization of the Universe in the mass range $10^{16} - 10^{17}$ g [37–39].

Gravitational lensing constraints

Gravitational lensing observations can be used to constrain the abundance of astrophysical objects within a mass range ranging from $10^{-10}M_\odot$ to $10^{8}M_\odot$. Among the most relevant observations we cite the search for PBH microlensing of stars lying in the Milky Way and M31 galaxy halo regions [40] which constraints the mass interval $10^{-10} < M < 10^{-6}M_\odot$, then other observations in the galactic halo from MACHO project and OGLE experiment whose combined results can be approximated to

$$f(M) < 1 \text{ for } 6 \times 10^{-8}M_\odot < M < 30M_\odot \tag{3.3.4}$$

$$f(M) < 0.1 \text{ for } 10^{-6}M_\odot < M < 1M_\odot \tag{3.3.5}$$

$$f(M) < 0.05 \text{ for } 10^{-3}M_\odot < M < 0.4M_\odot \, . \tag{3.3.6}$$

Then, JLA data was used in [41] to find the upper bound $f < 0.35$ for the mass range $10^{-2} < M < 10^{4}M_\odot$, but this limit could be weakened considering the option of an extended mass function or clustered PBHs.

Other important results come from quasar microlensing [42] which suggest a limit $f(M) < 1$ for $10^{-3} < M < 60M_\odot$, and millilensing of compact radio sources [43] that gives the limits:

$$f(M) < (M/2 \times 10^{4}M_\odot)^{-2} \text{ for } M < 10^{5}M_\odot \tag{3.3.7}$$

$$f(M) < 0.06 \text{ for } 10^{5}M_\odot < M < 10^{8}M_\odot \tag{3.3.8}$$

$$f(M) < (M/4 \times 10^{8}M_\odot)^{2} \text{ for } M > 10^{8}M_\odot \, . \tag{3.3.9}$$

Dynamical constraints

Dynamical constraints can be obtained from the study of the effects of collisions between PBHs and astronomical objects. For example, many authors have studied the possibility that PBHs could be captured by stars in the galactic disc [44], this leads to the lower mass limit

$$f < (M/3 \times 10^{26}\,\text{g}) \, . \tag{3.3.10}$$

Other limits on different mass ranges have been considered and disputed, so we do not report them here.

Further constraints come from the destruction of astrophysical objects caused by the passage of PBHs [45], considering multiple collisions, single collisions and non-impulsive encounters. These can be summed up in the following relation:

$$\frac{M_c v}{G\rho_{dm} t_L R_c} < M < M_c \left(\frac{v}{v_c}\right)^3 \tag{3.3.11}$$

where M_c is the object mass, v_c is its velocity dispersion and R_c is its radius, t_L is the survival time and v is the velocity dispersion of PBHs. The limit values correspond to values of M for which $f = 1$. Some examples of systems that are subject of these observations are wide binaries, globular clusters, dwarf galaxies, and also galaxy clusters (which cover PBHs that are too large to fit in a single galaxy halo).

Accretion constraints

Studying the effects on the Universe's thermal history, we observe that the accreting PBH radiates with luminosity [46]:

$$L = \epsilon \dot{M} c^2 \ . \tag{3.3.12}$$

This expression depends on the PBH mass and on the accretion specific dynamics, and the impact of the PBH on the Universe's temperature depends on the outgoing radiation. This outgoing flux can leave observable traces in the CMB, that can be used to derive bounds [47, 48]. These, however, are very model-dependent, and in the last years it has been observed that constraints could be less stringent than what was thought. Moreover, for smaller masses ($M \lesssim 10 M_\odot$) it is very difficult to constrain the abundance, because of the smaller impact of the PBHs on the surroundings.

Other constraints can be obtained by considering PBHs emission at the present epoch, particularly in the X-ray range, by studying the PBH contribution to the population of compact X-ray objects in galaxies. Relevant results have been obtained in [49, 50] and are shown in Fig. (3.1).

CMB constraints

The process of dissipation of post-inflationary gaussian density fluctuations by Silk damping can cause a $\mu-$distortion in the CMB spectrum, resulting in an upper limit on the overdensity

$$\delta(M) < \sqrt{\mu} \sim 10^{-2} \quad \text{for} \quad 10^3 < M/M_\odot < 10^{12} \ . \tag{3.3.13}$$

This turns in a constraint on $f(M)$, but relaxing the assumption that the fluctuations are gaussian may also weaken this constraint (though a very high degree of non-gaussianity would be needed).

The $\mu-$distortion limit also implies a maximum mass for dark matter PBHs, related to a limit on the steepness of the power spectrum in the theory of perturbations.

Gravitational wave constraints

As we reported before, recent years detections of gravitational waves by the LIGO/Virgo experiment prompted the rise of interest in PBHs. There are two ways in which gravitational waves could be related to PBHs: one is that a population of massive PBHs is expected to generate a gravitational wave background, that can be perturbed, in the present epoch, by binary BH coalescence; the second is from the tensor perturbations generated by scalar perturbations in the epoch of PBH formation, for which the frequency can be estimated and related to density perturbations, which in turn can be related to $f(M)$.

Early LIGO data gives strong limits to $f(M)$ in the mass range $0.5-30M_\odot$ [51], which are updated by more recent works [52–54] using more LIGO/Virgo data and pulsar-timing observations. The robustness of these bounds depends on the accuracy of the description of the PBH binaries formation. A 2018 estimate [55] gives a constraint on PBH fraction of dark matter $f \sim 0.001 - 0.01$.

Future observations by LISA could also detect stochastic emissions in the center of the Milky Way if PBHs of mass $10^{-13} - 1\,M_\odot$ were orbiting around a supermassive black hole in that region, forming a dark matter spike predicted in [56]. All of the constraints discussed in this section are graphically represented in Fig. (3.1) taken from Ref. [57]. In this graph, there are four interesting mass windows that are not constrained or are less constrained, that could be considered for PBH dark matter. In window C the gravitational-wave-related bounds are present, making it the most interesting window in light of recent developments. Window D, instead, contains a very high mass range, that would include the so-called SLABs (Stupendously Large Black Holes), that might provide an intergalactic dark matter component. Such massive PBHs are unlikely to form (they are in the tail of the overdensity distribution), however, by accretion, smaller PBHs could also reach that mass range.

3.3.2 Possibility of an extended mass function

In the previous discussion it was assumed that the mass function is monochromatic, meaning that PBHs are supposed to be generated all with the same mass. However, this scenario is very unlikely, and there are many methods to extend the limits for monochromatic mass functions to ones that have a non-negligible width ΔM.

We review here the approach used in [58, 59], where the authors introduce the function

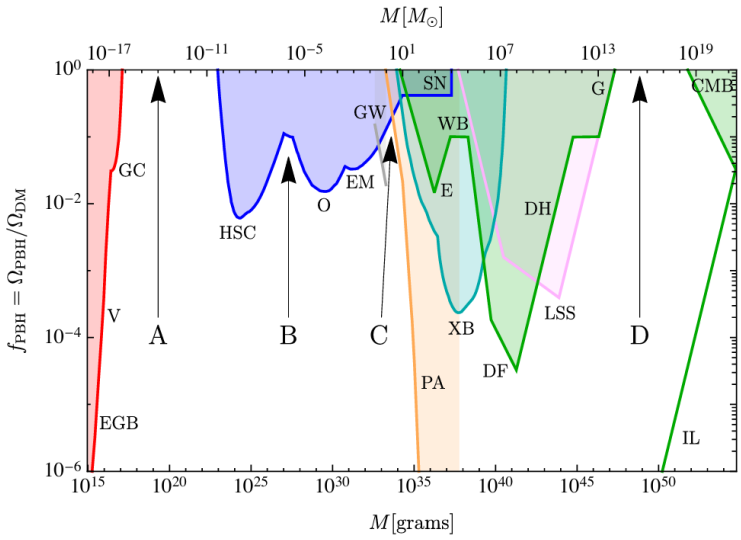

Figure 3.1: Constraints on $f(M)$ for a monochromatic mass function, from evaporations (red), lensing (blue), gravitational waves (GW) (gray), dynamical effects (green), accretion (light blue), CMB distortions (orange) and large-scale structure (purple). The incredulity limits (IL) correspond to one PBH per relevant environment (galaxy, cluster, Universe). There are four mass windows (A, B, C, D) in which PBHs could have an appreciable density.

$\psi(M)$ so that the total fraction (3.1.12) of dark matter in PBHs is

$$f_{pbh} = \int_{M_{min}}^{M_{max}} dM\, \psi(M)\ . \tag{3.3.14}$$

Any astrophysical observable depending on f_{pbh} can be expanded in the following way

$$A[\psi(M)] \simeq A_0 + \int dM\, \psi(M) K_1(M) + \int dM_1\, dM_2\, \psi(M_1)\psi(M_2)\, K_2(M_1, M_2)\ . \tag{3.3.15}$$

The constant A_0 is the background contribution, while K_1 and K_2 depend on the details of the physics related to the specific observable. If a measurement puts an upper bound on the observable:

$$A[\psi(M)] \leq A_{obs} \tag{3.3.16}$$

then, considering the case of a monochromatic mass function $\psi_{mc}(M) \equiv f_{pbh}(M_*)\delta(M - M_*)$, where $\log M_* \equiv \langle \log M \rangle_\psi$ is the mean of the logarithmic distribution, the maximum allowed fraction of PBH dark matter is

$$f_{pbh}(M_*) \leq \frac{A_{obs} - A_0}{K_1(M_*)} \tag{3.3.17}$$

which then yields:

$$\int dM \frac{\psi(M)}{f_{max}(M)} \leq 1 \ . \tag{3.3.18}$$

This equation can be applied in the case of an arbitrary mass function to obtain the relative constraints, provided that f_{max} is known. The result is a function of M_* and of the variance of the distribution $\sigma \equiv \sqrt{\langle \log^2 M \rangle_\psi - \langle \log M \rangle_\psi^2}$.

In references [58, 59], where the authors studied various mass functions, the general result is that the allowed mass range for fixed value of f_{pbh} decreases when the width σ of the mass function increases. There are also more complicated scenarios that generally require more parameters, however a study of such models would be beyond the scope of this thesis.

Chapter 4

Jordan frame formalism

This chapter's purpose is that of establishing the theoretical framework for studying inflationary models in two different frames, namely the Jordan frame and the Einstein frame. The two frames are connected by a frame transformation, which affects the inflationary formalism. We first present the transformation, then we discuss how important expressions for inflationary dynamics are modified, and how the conditions that define different inflationary regimes change. We will explore the two regimes that we consider important in this analysis, namely the slow-roll and ultra-slow-roll regimes.

4.1 Dynamics in the Jordan frame

We will start with an introduction on the concept of Jordan frame. The Jordan frame was first introduced in the context of general scalar-tensor theories as the frame in which the Lagrangian contains a term where the scalar field is coupled non-minimally to the Ricci scalar. In the context of inflation, many theories have been studied in the literature having this non-minimal coupling term between the inflaton and gravity, and the transformations between Jordan and Einstein frames are essential in order to study these theories.

The inflaton action (1.7.1) in Jordan frame has the following generic form:

$$S_J = \int d^4x\sqrt{-g}\left[-U(\sigma)R + \frac{1}{2}g^{\mu\nu}\sigma_{,\mu}\sigma_{,\nu} - V(\sigma)\right] \tag{4.1.1}$$

where the function $U(\sigma)$ describes the non-minimal coupling of the field to gravity.

It is important to show how the Friedmann and Klein-Gordon equations change in form, and how the conditions for slow-roll and ultra-slow-roll map between the two frames, so that we can adapt the requirements for inflation and non-slow-roll regimes in Einstein frame to the more generic non-minimally coupled case.

By varying the action (4.1.1), the resulting equations are:

$$6UH^2 + 6\dot{U}H = \frac{\dot{\sigma}^2}{2} + V\,, \tag{4.1.2}$$

$$2U(2\dot{H} + 3H^2) + 4\dot{U}H + 2\ddot{U} + \frac{\dot{\sigma}^2}{2} - V = 0\,, \tag{4.1.3}$$

$$\ddot{\sigma} + 3H\dot{\sigma} + V_{,\sigma} = 6(\dot{H} + 2H^2)U_{,\sigma}\,. \tag{4.1.4}$$

The homogeneous equations for the inflaton-gravity system in the Jordan frame are more cumbersome, due to the extra field dependence. The exact resolution of the system is often equally cumbersome, therefore in many cases, authors choose to switch from the Jordan frame to the Einstein frame, where the formalism is usually more suitable to computations.

To go from the Jordan frame to the Einstein frame, it is necessary to perform a conformal (Weyl) transformation of the metric in the following way:

$$g_{\mu\nu} = \frac{U_0}{U(\sigma)}\tilde{g}_{\mu\nu}\,. \tag{4.1.5}$$

With this transformation, the term in the action containing R becomes the canonical term $U_0\tilde{R}$, where the constant is the usual $U_0 = M_P^2/2$. As for the kinetic term, we have to perform another transformation to obtain the canonical kinetic term through the field redefinition defined by:

$$\frac{d\phi}{d\sigma} = \frac{\sqrt{U_0(U(\sigma) + 3U(\sigma)^2_{,\sigma})}}{U(\sigma)} \tag{4.1.6}$$

where ϕ is the field in the Einstein frame. After these two changes, the potential is redefined as:

$$W(\phi) = \frac{U_0^2 V(\sigma(\phi)}{U^2(\sigma(\phi))}\,. \tag{4.1.7}$$

The action in the Einstein frame becomes:

$$S_E = \int d^4x\sqrt{-\tilde{g}}\left[-U_0\mathcal{R} + \frac{1}{2}\tilde{g}_{\mu\nu}\partial^\mu\phi\,\partial^\nu\phi - W(\phi)\right] \tag{4.1.8}$$

which corresponds to (1.7.1) in a different notation, and the equations of motion for this action are (1.7.2), (1.7.3) and (1.7.4).

Before proceeding, we introduce a definition that will be useful in the rest of the thesis:

$$n_f(\sigma) \equiv \frac{\sigma f_{,\sigma}}{f}\,. \tag{4.1.9}$$

We then introduce the field functions $n_U = \sigma U_{,\sigma}/U$, $n_{n_U} = \sigma n_{U,\sigma}/n_U$, and we can define,

in a similar way for V, the functions $n_V = \sigma V_{,\sigma}/V$, $n_{n_V} = \sigma n_{V,\sigma}/n_V$. The advantage in using these functions is that the notation gets lighter, especially in more advanced calculations, and in some models we can assume these functions as constants, at least approximately.

Equations (4.1.2), (4.1.3) and (4.1.4) can be written in terms of the SR parameters and of the functions defined by (4.1.9), by substituting them where possible. What we obtain is:

$$H^2 = \frac{V}{6U\left(1 + n_U\delta_1 - \frac{\sigma^2}{12U}\delta_1^2\right)} \tag{4.1.10}$$

$$\varepsilon_1 = \frac{n_U\delta_1(\delta_2 + n_{n_U}\delta_1 + n_U\delta_1 - 1) + \frac{\sigma^2}{2U}\delta_1^2}{2 + n_U\delta_1} \tag{4.1.11}$$

$$\frac{\sigma^2}{U}\delta_1(\delta_1 + \delta_2 - \varepsilon_1 + 3) + \frac{V}{H^2U}n_V = 6n_U(2 - \varepsilon_1)\,. \tag{4.1.12}$$

Starting from these equations, we can perform some useful calculations in the Jordan frame in order to express the SR parameters, in slow-roll approximation, as functions of the field alone. In slow-roll regime, all the SR parameters are considered small, hence we can neglect terms of order 2 in the parameters ($\sim \delta_i\delta_j$). If the quantity $\frac{\sigma^2}{U}$ is $\mathcal{O}(1)$ and n_f is not too large, the second equation in (4.1.10) becomes, under SR approximation:

$$\varepsilon_1 \simeq -\frac{n_U\delta_1}{2}\,. \tag{4.1.13}$$

By substituting the first and second equation into (5.1.12), we obtain this form for the Klein-Gordon equation:

$$\frac{\sigma^2}{6U}\delta_1(\delta_1 + \delta_2 + 1) + n_V\left(1 + n_U\delta_1 - \frac{\sigma^2}{12U}\delta_1^2\right) =$$

$$= \left(n_U - \frac{\sigma^2}{6U}\delta_1\right)\left[2 - \frac{n_U\delta_1(\delta_2 + n_{n_U}\delta_1 + n_U\delta_1 - 1) + \frac{\sigma^2}{2U}\delta_1^2}{2 + n_U\delta_1}\right]$$

Applying the slow-roll approximation, we obtain the following expression for δ_1:

$$\delta_1 \simeq \frac{2n_U - n_V}{\frac{\sigma^2}{2U} + n_U(n_V - n_U/2)} \tag{4.1.14}$$

4.2 Slow-roll and ultra-slow-roll conditions

To discuss how the conditions for slow-roll and other regimes change between frames, we have to relate the SR parameters in Jordan and Einstein frames. We start from writing the scale factor a and the lapse function n, which in the Einstein frame become:

$$\tilde{a} = \sqrt{\frac{U}{U_0}}\, a \tag{4.2.1}$$

$$\tilde{n} = \sqrt{\frac{U}{U_0}}\, n \tag{4.2.2}$$

where $U = U(\sigma(\phi))$.

From the equations (4.2.1), we can easily find the Hubble parameter:

$$\tilde{H} = \sqrt{\frac{U_0}{U}} \left(1 + \frac{n_U}{2}\delta_1\right) H \tag{4.2.3}$$

and also the number of e-folds:

$$\tilde{N} = \ln \tilde{a} = \frac{1}{2}(\ln U - \ln U_0) + N\,. \tag{4.2.4}$$

The fact that the number of e-folds changes between frames shows that the frame transformation affects the physical meaning of inflationary scenarios. The length of inflation, as well as the length of the transient USR period, are important quantities that are constrained by observations.

To derive the slow-roll parameters in the Einstein frame, it is useful to find the expression $d\tilde{N}/dN$:

$$\frac{d\tilde{N}}{dN} = 1 + \frac{n_U \delta_1}{2}\,. \tag{4.2.5}$$

Now we can easily derive the expression for the first slow-roll parameter:

$$\tilde{\varepsilon}_1 \equiv -\frac{d\ln\tilde{H}}{d\tilde{N}} = \left(1 + \frac{n_U\delta_1}{2}\right)^{-1} \left[\frac{n_U\delta_1}{2} + \varepsilon_1 - \frac{\frac{n_U\delta_1}{2}(n_{n_U}\delta_1 + \delta_2)}{1 + \frac{n_U\delta_1}{2}}\right] \tag{4.2.6}$$

and by directly differentiating the former expression with respect to $\tilde{N}$, one obtains the second slow-roll parameter:

$$\tilde{\varepsilon}_2 \equiv \frac{\delta_1\left[6n_{n_U}n_U^2 + \frac{\sigma^2}{U}(2 - n_U)\right]}{\left(3n_U^2 + \frac{\sigma^2}{U}\right)\left(1 + \frac{n_U\delta_1}{2}\right)} + \frac{2\delta_2}{\left(1 + \frac{n_U\delta_1}{2}\right)} - \frac{n_U\delta_1(n_{n_U}\delta_1 + \delta_2)}{\left(1 + \frac{n_U\delta_1}{2}\right)^2}\,. \tag{4.2.7}$$

These relations are sufficient to exactly map the slow-roll and ultra-slow-roll conditions from one frame to the other, as we shall explain in what follows:

1. The slow-roll conditions in the Einstein frame are:

$$\tilde{\varepsilon}_1 \approx \tilde{\varepsilon}_2 \ll 1\,. \tag{4.2.8}$$

   Assuming that the functions n_U and n_{n_U} are of order $\mathcal{O}(1)$, looking at expression (4.2.6), this is equivalent to assuming $\delta_1 \approx \varepsilon_1 \ll 1$, while looking at (4.2.7) slow-roll implies $\delta_1 \approx \delta_2 \ll 1$. By further differentiating to find the successive slow-roll parameters, it is possible to verify that if all the SR parameters in the Einstein frame are small, then all the parameters in the Jordan frame have to be small as well and viceversa. We can conclude that the slow-roll condition is the same in the two frames.

2. For ultra-slow-roll, we can start by imposing $\tilde{\varepsilon}_1 \ll 1$, as in the former case, and this implies once again $\delta_1 \approx \varepsilon_1 \ll 1$. For the second parameter $\tilde{\varepsilon}_2$, Eq. (4.2.7) reduces to

$$\tilde{\varepsilon}_2 \simeq 2\delta_2\,. \tag{4.2.9}$$

   Given the condition for ultra-slow-roll (2.4.8) that we derived in Chapter (2), we obtain the following condition for the parameter δ_2:

$$\delta_2 \simeq -3\,. \tag{4.2.10}$$

Another important definition that changes when considering the Jordan frame is that of the pump field z (2.2.3). Indeed, considering the modifications (4.2.1), (4.2.3) and the change of field (4.1.6), the expression of the pump field becomes:

$$z \equiv \tilde{a}\frac{\dot{\phi}}{\tilde{H}} = \frac{\sqrt{1+3\frac{\dot{U}^2}{\dot{\sigma}^2 U}}}{1+\frac{\dot{U}}{2HU}}\frac{a\dot{\sigma}}{H} \tag{4.2.11}$$

This expression will be important when numerically computing the power spectrum of perturbations in a non-minimally coupled scalar field model.

4.3 Observable quantities in perturbations theory

Finally, we consider the transformations of the quantities related to the study of the perturbations spectrum. We first look at how the spectrum amplitude is related to the slow-roll parameters. Starting from expression (2.2.17)

$$\mathcal{P}_{\mathcal{R}}(k) = \left[\frac{H^4}{4\pi^2\dot{\phi}^2}\right]_{k=aH} . \tag{4.3.1}$$

In slow-roll approximation this can be written in the Einstein frame as

$$\mathcal{P}_{\mathcal{R}} \simeq \frac{W}{24\pi^2 M_P^4 \tilde{\varepsilon}_1} = \frac{W}{12\pi^2 M_P^2 \phi^2 \tilde{\delta}_1^2} . \tag{4.3.2}$$

To explain the second equality, we take the second equation in (4.1.10) and write it in the Einstein frame ($n_U = n_{n_U} = 0$):

$$\tilde{\varepsilon}_1 = \frac{\sigma^2 \tilde{\delta}_1^2}{4U} \tag{4.3.3}$$

Substituting this expression in that for $\mathcal{P}_{\mathcal{R}}$, and considering the Einstein frame minimal coupling $U = U_0 = M_P^2/2$ we obtain the result (4.3.2).

Now, using the expression for $\tilde{\varepsilon}_1$ in terms of Jordan frame parameters, and substituting the Jordan frame SR parameters so that the expression is only a function of the field, we can write the spectrum as

$$\mathcal{P}_{\mathcal{R}} \simeq \frac{V}{12\pi^2 U \sigma^2 (1 + 3n_U^2 \frac{U}{\sigma^2})} \left[\frac{\frac{\sigma^2}{2U} + n_U(n_V - n_U/2)}{2n_U - n_V}\right] . \tag{4.3.4}$$

This formula for the spectrum will provide an analytic result assuming the SR approximation.

The other interesting quantity to look at is the scalar spectral index (2.1.51), in particular we are interested in the CMB scales, and the long wavelength limit (small k/aH). We derive an approximate expression at these scales, starting from the equation of motion for scalar perturbations (2.2.2), and rewriting it in terms of the slow-roll parameters:

$$\zeta^2 \frac{\mathrm{d}^2\mathcal{R}_k}{\mathrm{d}\zeta^2} + \left[\frac{\varepsilon_1\varepsilon_2 - 2(1-\varepsilon_1)\frac{\mathrm{d}\ln z}{\mathrm{d}N}}{(1-\varepsilon_1)^2}\right] \zeta \frac{\mathrm{d}\mathcal{R}_k}{\mathrm{d}\zeta} + \frac{\zeta^2}{(1-\varepsilon_1)^2}\mathcal{R}_k = 0 \tag{4.3.5}$$

where $\zeta \equiv k/(aH)$. The long wavelength limit corresponds to $\zeta \to 0$, and in this limit, assuming constant slow-roll parameters, Eq. (4.3.5) admits a solution of the form

$$\mathcal{R}_k \simeq e^{-B(1-\varepsilon_1)N} \tag{4.3.6}$$

with

$$B = 1 - \frac{\varepsilon_1\varepsilon_2 - 2(1-\varepsilon_1)\frac{\mathrm{d}\ln z}{\mathrm{d}N}}{(1-\varepsilon_1)^2} . \tag{4.3.7}$$

In this case, the scalar spectral index has the following expression:

$$n_s - 1 = 2 - \left[\frac{\varepsilon_1\varepsilon_2}{(1-\varepsilon_1)^2} - 1\right] - \sqrt{\left[\frac{\varepsilon_1\varepsilon_2}{(1-\varepsilon_1)^2} - 1\right]^2 + 4\frac{z_{,NN} + (1-\varepsilon_1)z_{,N}}{z(1-\varepsilon_1)^2}}\,. \tag{4.3.8}$$

Now we can consider equations (4.2.11) and (4.1.10) in order to eliminate the dependence from z and ε_2, and considering the slow-roll limit (where the CMB scale exits the horizon), we obtain the following expression for $n_s - 1$:

$$n_s - 1 \simeq -2(\delta_1 + \delta_2 + \varepsilon_1) + \frac{3n_U^2\delta_1(2 - n_U - 2n_{n_U})}{3n_U^2 + \frac{\sigma^2}{U}}\,. \tag{4.3.9}$$

We can also calculate the expression of another important observable, the tensor-to-scalar ratio r (2.1.52) in slow-roll regime, by using the relation between scalar and tensor spectra (2.2.24). The result is:

$$r = 2\sigma^2\delta_1^2\frac{\left(1 + 3n_U^2\frac{U}{\sigma^2}\right)}{U}\,. \tag{4.3.10}$$

Chapter 5

PBHs production in Higgs inflation

In this chapter, we examine an inflationary scenario in which the Higgs boson plays the role of the inflaton, within a framework that includes a non-minimal coupling between the inflaton and the Ricci scalar. This model has been first proposed by Bezrukov and Shaposhnikov in 2007 [5] with the aim of matching the model parameters with the CMB measurements, as well as the Standard Model results for the Higgs boson mass and quartic self-coupling.

In the first section of this chapter, we first provide an overview of the original Higgs inflation model, and we follow with the study of the framework of critical Higgs inflation, in which an inflection point is considered in the Higgs field potential. With the right tuning of the parameters, this model could lead to amplifications of the curvature power spectrum eligible for PBH production. We will reference [60] in this discussion.

In the second section, we consider an original model of Higgs inflation formulated directly in the Jordan frame, where the physical potential is defined. We present the proposed model, explaining the performed analysis of the relevant expressions and parameters, and the obtained results.

5.1 Higgs inflation in Einstein frame

5.1.1 Original model

In this section we review the original model of Higgs inflation. proposed by Bezrukov and Shaposhnikov in [5] and further elaborated in [6]. The primary reason to consider the Higgs boson as the inflaton is that it would eliminate the need to introduce a new field, since the Higgs boson is already well integrated in the Standard Model. Moreover, Planck data shows that single-field models such as Higgs inflation are favoured over multi-field ones. This model can be easily generalized to a generic inflation field by not constraining

the self-coupling to be the Higgs one.

The original model formulation of Higgs inflation includes a non-minimal coupling to gravity. The action in the Jordan frame is given by:

$$S_{Higgs} = \int d^4x\sqrt{-g}\left(-\frac{M_P^2+\xi h^2}{2}R + \frac{1}{2}g_{\mu\nu}\partial^\mu h\partial^\mu h - \frac{\lambda}{4}(h^2-v^2)^2\right) \tag{5.1.1}$$

where ξ is the non-minimal coupling constant and λ denotes the quartic self-coupling. The model is an example of large-field inflation with a chaotic inflation polynomial potential. If the model didn't include the non-minimal coupling, given the large field excursion, the quartic self-coupling in the potential would have to be small in order to maintain the flatness of the potential and suppress radiative corrections that could otherwise spoil the slow-roll conditions. Typically, the requirement is $\lambda \lesssim 10^{-12}$. The value of λ at the Planck scale calculated at tree level is $\lambda = 0.129$ and does not satisfy this bound, so the non-minimal coupling to gravity is introduced to compensate for the large value of λ. Indeed, we will see that the constraint on the Higgs self-coupling contains the parameter ξ, so λ can be any value.

The non-minimal coupling to gravity is quadratic in the Higgs field and leads to an effective change of the Planck mass $M_{P,eff}^2 \sim M_P^2 + \xi h^2$. After inflation, assuming that the minimum of the inflaton potential is at $h \sim 0$, the effective Planck mass returns to its standard value, $M_{P,eff}^2 = M_P^2$.

Following ref. [6], we can perform a conformal transformation to transition from the Jordan frame to the Einstein frame. Such transformation is defined by:

$$\hat{g}_{\mu\nu} = \Omega^2 g_{\mu\nu} \tag{5.1.2}$$

where the conformal factor is

$$\Omega^2 = 1 + \frac{\xi h^2}{M_P^2}\,. \tag{5.1.3}$$

Combining this transformation with a redefinition of the scalar field according to (4.1.6), we obtain the following action in the Einstein frame:

$$S_{H,E} = \int d^4x\sqrt{-\hat{g}}\left(-\frac{M_P^2}{2}\hat{R} + \frac{\hat{g}_{\mu\nu}\partial^\mu\chi\partial^\mu\chi}{2} - U(\chi)\right) \tag{5.1.4}$$

where χ is the new field in the Einstein frame and, according to (4.1.7), the Einstein frame potential is

$$U(\chi) = \frac{1}{\Omega^4(\chi)}\,\frac{\lambda}{4}(h(\chi)^2 - v^2)^2\,. \tag{5.1.5}$$

Higgs inflation is characterized by a large non-minimal coupling $\xi \gg 1$ and a negligible

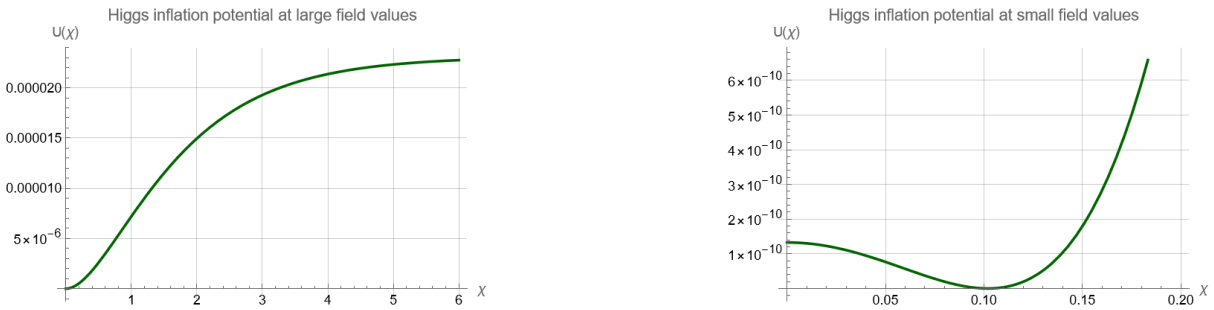

Figure 5.1: Characteristic form of Higgs inflation potential seen from two interesting scales of the field values, for the choice of parameters $\lambda = 0.129$ and $v = 0.102$

vacuum contribution of the non-minimal coupling to the effective Planck mass. In this case, the potential in the Einstein frame takes the form:

$$U(\chi) = \begin{cases} \frac{\lambda M_P^4}{4\xi^2}\left(1 - \mathrm{e}^{-\frac{2\chi}{\sqrt{6}M_P}}\right)^2, & \chi \gg M_P/\xi \\ \frac{\lambda}{4}(\chi^2 - v^2)^2, & \chi \ll M_P/\xi \end{cases} \tag{5.1.6}$$

At large field values, the potential becomes flat, providing the necessary conditions for slow-roll inflation, while for small field values, the potential becomes the SM Higgs boson quartic potential with a negative mass. The characteristic shape of the potential (5.1.5) is shown in the Figure (5.1), with parameters $\lambda = 0.129$, $v = 0.102$, and $\xi = 16\,880.8$.

In the slow-roll regime, the SR parameter ε_1 can be easily expressed as a function of the Higgs field h:

$$\varepsilon_1 \simeq \frac{4M_P^4}{3\xi^2 h^4}\,. \tag{5.1.7}$$

Considering that inflation ends at $\varepsilon_1 \simeq 1$, the field value at the end of inflation is $h_{end} \simeq (4/3)^{1/4} M_P/\sqrt{\xi} \simeq 1.07 M_P/\sqrt{\xi}$. We can calculate the number of e-folds as a function of h:

$$N = \int_{h_{end}}^{h_N} \frac{U\chi'^2}{M_P^2 U'}\mathrm{d}h \simeq \frac{3}{4}\left[\left(\xi + \frac{1}{6}\right)\frac{h_N^2 - h_{end}^2}{M_P^2} - \ln\frac{(1 + \frac{\xi h_N^2}{M_P^2})}{(1 + \frac{\xi h_{end}^2}{M_P^2})}\right]\,. \tag{5.1.8}$$

This relation allows one to identify the field value $h(N)$ at which a given mode, associated with N, exits the horizon. In particular, the modes imprinted in the CMB cross the horizon when $h_{cmb} \simeq 9.14 M_P/\sqrt{\xi}$. Using the observed amplitude of the scalar power spectrum $\mathcal{P}_\mathcal{R}$ at CMB scales, and the expression of the spectrum obtained with the SR approximation (4.3.2), we can deduce that the following condition needs to be satisfied at h_{cmb}:

$$U/\varepsilon_1 \simeq (0.0276\, M_P)^4\,. \tag{5.1.9}$$

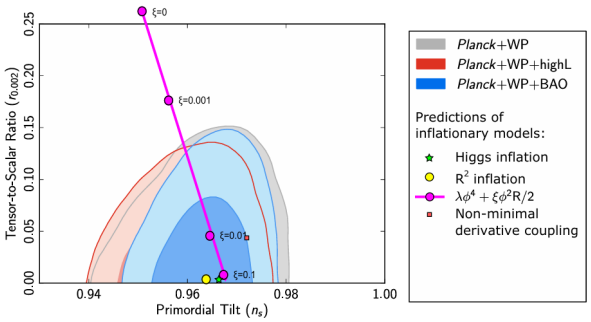

Figure 5.2: In this plot from ref. [6], the results for n_s and r are shown for Higgs inflation and Higgs inflation-inspired models, along with experimental data from the Planck satellite.

This means that the non-minimal coupling ξ is constrained by the following relation:

$$\xi \simeq 47000\sqrt{\lambda}\,. \tag{5.1.10}$$

For suitable values of ξ and λ, this model yields inflationary observables in agreement with current cosmological data. For the Higgs SM quartic coupling at tree level ($\lambda = 0.129$), to the lowest order in $1/\xi$, the spectral index and the tensor-to-scalar ratio are:

$$n_s - 1 \simeq 0.967 \tag{5.1.11}$$

$$r \simeq 0.0031 \tag{5.1.12}$$

This is shown in Fig. (5.2) (the green star marker at the bottom). In the same figure, the pink straight line marks the values of ξ and λ that obey the relation (5.1.10). There exists a parameter range in which the values of r and n_s remain within observational bounds, suggesting that the Higgs inflation scenario could also be realized with a generic scalar field acting as the inflaton, rather than the Higgs field.

An important consequence of identifying the Higgs boson with the inflaton is that the mechanism of preheating is effectively fixed by the Standard Model interactions. After inflation ends, the Higgs field oscillates around the electroweak vacuum, efficiently producing SM particles, primarily W and Z bosons. Once parametric resonance becomes efficient, these gauge bosons live long enough to decay into lighter SM particles, leading to thermalization of the universe.

The main shortcoming of Higgs inflation is that the theory is not UV-complete, meaning that it has a strong scale dependence. The effective theory breaks down at an energy scale $\Lambda \sim M_P/\xi$, below the inflationary Hubble scale for large ξ. This implies a violation of tree-level unitarity during inflation, unless new physics enters before this cutoff [61].

5.1.2 Critical Higgs inflation

The scenario of Higgs inflation was initially considered with the primary goal of matching observations at CMB scales. However, more recent articles have explored the possibility that quantum corrections to the Higgs potential could lead to features in the power spectrum that might lead to the formation of primordial black holes. In this section, we focus on the scenario of critical Higgs inflation, following in particular the analysis presented in [60, 62].

The idea of critical Higgs inflation stems from the observation that quantum radiative corrections can change the form of the effective potential, modifying the inflationary dynamics and therefore the predictions of Higgs inflation.

From the analysis of quantum effects at 2-loop level in ref. [63], it emerges that the stability of the SM vacuum at the electroweak scale depends, among other parameters, on the Higgs mass M_h. The stability condition is that the Higgs mass has to be above a certain value:

$$M_{crit} = \left(129.6 + 2\frac{y_t^{phys} - 0.9361}{0.0058} - 0.5\frac{\alpha_s - 0.1184}{0.0007} \right) \text{GeV} \tag{5.1.13}$$

where y_t^{phys} is the coupling of h to the top quark t and α_s is the coupling to the Z gauge boson. When the Higgs mass is above M_{crit} by at least $\mathcal{O}(100\,\text{MeV})$, the values of cosmological parameters are rather stable, and Higgs inflation is a good inflationary scenario at CMB scales. The situation is different when M_h approaches M_{crit}. In fact, in this case, the running of λ

$$\lambda(z) = \lambda_0 + b_\lambda (\ln z)^2 \tag{5.1.14}$$

and of its beta function

$$\beta_\lambda = \mu \frac{\partial \lambda}{\partial \mu} \tag{5.1.15}$$

where all the parameters are functions of y_t^{phys} and α_s, approach zero near the Planck scale, and this considerably changes the effective potential, as well as the behavior of the inflationary parameters [62]. Without going into details about this mechanism, the result is that, near the critical point, an inflection point, or even a local minimum, appears in the potential. The presence of an inflection point considerably opens up the parameter space. As shown in Fig. (5.3) from ref. [62], the (n_s, r) predictions are no longer confined to a narrow line, as in standard Higgs inflation (5.2), but can span a much wider region of the observationally allowed parameter space.

Considering the critical Higgs inflation would also solve the problem related to unitarity at Planck scales. Indeed, given the small value of $\lambda(z)$ in this scenario, the electroweak vacuum stability is preserved without requiring a large value of ξ, raising the cutoff scale

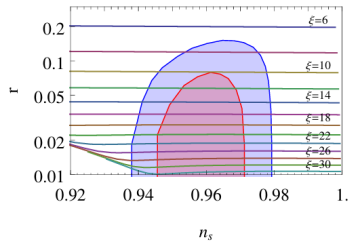

(a) Dependence on the inflationary parameters on ξ and k, a grid of lines of constant ξ and varying k is shown

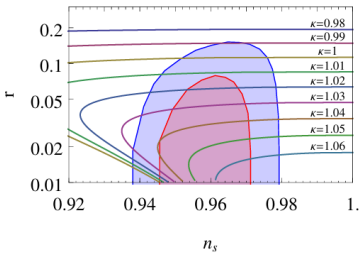

(b) Same dependence but with the grid of constant k, varying ξ

Figure 5.3: Results from the analysis of critical inflation in ref. [62]

of the theory.

In article [60], the previous analysis is extended by considering the possibility that the non-minimal coupling ξ is also subjected to changes in function of the Higgs mass. Consider the running of both parameters λ and ξ, expanded around the critical point $h = \mu$ that corresponds to the critical mass M_{crit}:

$$\lambda(h) = \lambda_0 + b_\lambda \ln^2(h/\mu) \tag{5.1.16}$$

$$\xi(h) = \xi_0 + b_\xi \ln(h/\mu)\,. \tag{5.1.17}$$

The effective potential in the Einstein frame in this case becomes

$$U(x) = \frac{U_0(1 + a\,\ln^2 x)\,x^4}{(1 + c(1 + b\,\ln x)\,x^2)^2} \tag{5.1.18}$$

where the rescaled parameters are defined by:

$$U_0 = \lambda_0\mu^4/4, \quad a = b_\lambda/\lambda_0, \quad b = b_\xi/\xi_0, \quad c = \xi_0\mu^2/M_P^2\,. \tag{5.1.19}$$

The presence of an inflection point at $x = x_c$ requires that both first and second derivative of the potential vanish, $V'(x_c) = V''(x_c) = 0$. Imposing these conditions on the potential

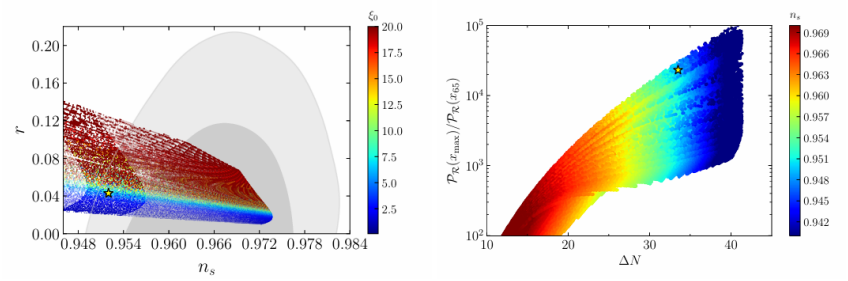

Figure 5.4: Results from ref. [60]

(5.1.18) gives the following relations between parameters:

$$a(x_c, c) = \frac{4}{1 + cx_c^2 + 2\ln x_c - 4\ln^2 x_c}\,, \tag{5.1.20}$$

$$b(x_c, c) = \frac{2(1 + cx_c^2 + 4\ln x_c + 2cx_c^2 \ln x_c)}{cx_c^2(1 + cx_c^2 + 2\ln x_c - 4\ln^2 x_)}\,. \tag{5.1.21}$$

A quasi-inflection point is obtained by correcting the parameter b by a small factor, $b \to (1-\beta)b(x_c, c)$. This correction makes it easy to control the length ΔN of the period in which the inflaton rolls down the now quasi-inflection point by tuning β (this length is inversely proportional to β).

The results of the study of the parameter space $(x_c, c, \beta, \Delta N)$ show that there are several parameters that match cosmological observables at CMB scales, but do not provide sufficient amplification of the spectrum. Furthermore, to obtain sufficient amplification, it appears that the number of e-folds ΔN spent around the inflection point has to be at least greater than 40, which is too long to be compatible with any model including CMB constraints, in fact these cases appear to predict a low spectral index ($n_s < 0.956$) and a large tensor-to-scalar ratio ($r > 0.019$).

5.2 Higgs inflation in Jordan frame

In this section, we present an inflationary scenario inspired by Higgs inflation, but where the physical potential is defined directly in the Jordan frame. In particular, we consider the following expression for the potential:

$$V(h) = \frac{\lambda}{4}h^4(1 + v_2 h^2 + v_4 h^4)\,. \tag{5.2.1}$$

This potential becomes the Higgs quartic potential for small field values, and for simplicity we neglect $v = \langle h \rangle$. Two correction terms of order $\sim h^6$ and $\sim h^8$ have been added in order to introduce new features in the potential. For the non-minimal coupling, we consider the expression

$$U(h) = \frac{1}{2}(M_P^2 + u_2 h^2 + u_4 h^4) \tag{5.2.2}$$

introducing an additional term $\sim h^4$ with respect to the Bezrukov model in [6]. This addition is necessary in the presence of the extra terms in the potential V because these contributions together ensure that V/U^2 is approximately constant in the large field limit. This is necessary in order to obtain quasi-de Sitter solutions in the Jordan frame, in analogy with the Einstein frame case requiring $W \sim$ constant .

We focus on scenarios in which the Einstein frame potential $W(h) = V/U^2$ exhibits an inflection point at $h = h_0$. For simplicity, from this point forward we will consider $M_P = 1$. By imposing

$$W'(h_0) = 0 \ , \ W''(h_0) = 0 \, , \tag{5.2.3}$$

which in terms of U and V are equivalent to

$$2n_U(h_0) = n_V(h_0) \, , \quad n_{n_U}(h_0) = n_{n_V}(h_0) \, , \tag{5.2.4}$$

we can express v_2 and v_4 in terms of u_2, u_4 and h_0:

$$v_2 = -\frac{2(4 + 3u_2 h_0^2 + u_2 u_4 h_0^6)}{h_0^2(6 + 6u_2 h_0^2 + (u_2^2 + 2u_4)h_0^4)} \ , \tag{5.2.5}$$

$$v_4 = \frac{3 + 2u_2 h_0^2 + u_4^2 h_0^8}{h_0^4(6 + 6u_2 h_0^2 + (u_2^2 + 2u_4)h_0^4)} \, . \tag{5.2.6}$$

As a result, V and U only depend on the three parameters u_2, u_4 and h_0, along with λ. These are the parameters that will be adjusted to produce the desired power spectrum.

Following expressions (4.3.4) and (4.3.9), we have searched for parameters that match the value of $\mathcal{P}_\mathcal{R}$ and $n_s - 1$ at CMB scales. These correspond, according to measurements [64], to:

$$\mathcal{P}_\mathcal{R} \simeq 2.2 \times 10^{-9} \tag{5.2.7}$$

and

$$n_s \simeq 0.9641 \pm 0.0044 \, . \tag{5.2.8}$$

An example of how such matching is searched for is illustrated in figures (5.5) and (5.6). In Figure (5.6) one can notice two horizontal colored lines. These represent the experimental bounds on the quantity n_s within 3σ. Since it has been observed that the scalar spectral index value tends to be redshifted (typically $n_s \sim 0.950$) when the 7-order magnitude

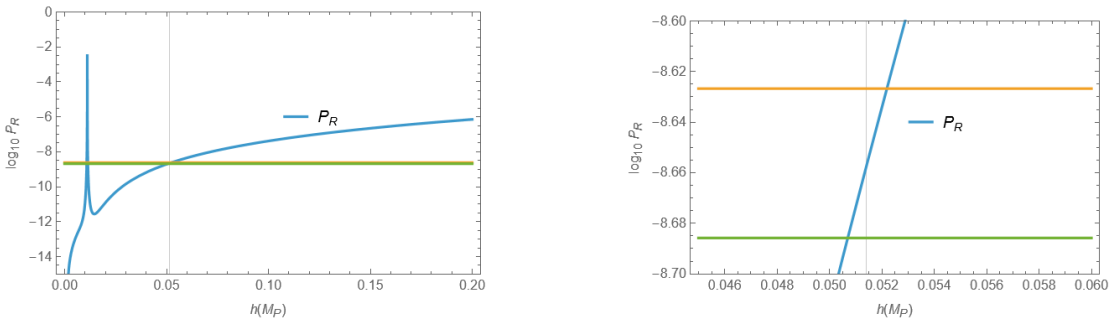

Figure 5.5: Plot of the approximated power spectrum expression (4.3.2) as function of the field, with the choice of parameters $u_2 = -10^{-6}$, $u_4 = 3.50752 \times 10^7$, $h_0 = 0.0110917$ and $\lambda = 0.129$. On the left, the entire field range covered during inflation is showed; the horizontal lines correspond to the experimental boundaries to the quantity $\mathcal{P}_{\mathcal{R}}(k_{cmb})$, while the vertical line marks the value of the field where the exiting k mode has an amplitude at horizon exit that corresponds to $\mathcal{P}_{\mathcal{R}}(k_{cmb})$. The power spectrum intersects the vertical line within the required boundaries, as shown on the right, where the plot around the intersection is magnified.

amplification is realized, we search for the match in the lower half of the band delimited by the two horizontal lines.

At the same time, we can plot the slow-roll approximation of the parameter ε_1, expression (4.1.13), to see if the fundamental condition for inflation, $\varepsilon_1 \ll 1$, is satisfied throughout the field excursion. We suppose that inflation will start around the point in which the potential W starts to slowly decrease. The exact initial conditions for the field value do not have to be finely tuned, as the slow-roll inflation regime is an attractor for the field dynamics.

To obtain amplification of the scalar spectrum, we are interested in the value of the parameter δ_2. Our target value during the transient phase is $\delta_2 \simeq -3$, as we have seen in section (4) while discussing the condition for ultra-slow-roll regime.

To ensure that the intermediate phase lasts for an appropriate amount of e-folds, we have to consider the relative importance of the friction and acceleration terms in the Klein-Gordon equation, and how they affect the inflaton dynamics. Consider the Klein-Gordon equation in the ultra-slow-roll regime (2.4.5):

$$\ddot{\phi} + 3H\dot{\phi} \simeq 0\,. \tag{5.2.9}$$

For a successful ultra-slow-roll phase, it is important that the field passes through the inflection point, and this can happen if the velocity of the field at the beginning of the USR phase is not too small. However, if the velocity is too large, the inflaton could get through the USR plateau too fast, meaning that the ultra-slow-roll epoch would be too small. The dynamics of the slow-roll phase therefore plays an important role in the realization of the desired amplifications.

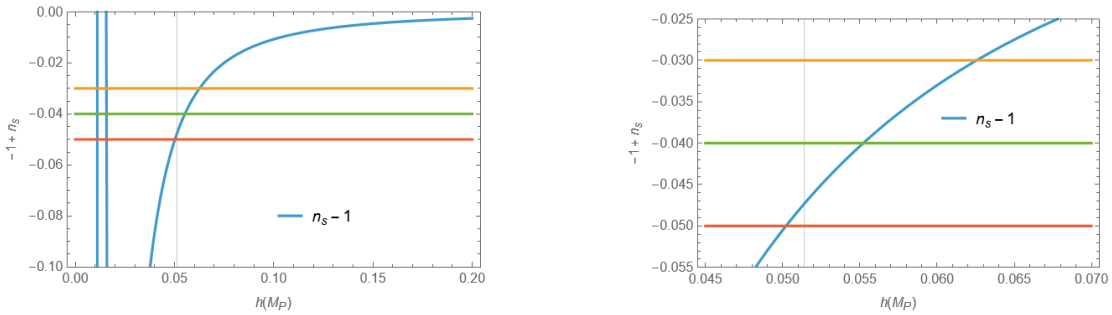

Figure 5.6: Plot of the scalar spectral index n_s as function of the field (in blue), with the choice of parameters $u_2 = -10^{-6}$, $u_4 = 3.50752 \times 10^7$, $h_0 = 0.0110917$ and $\lambda = 0.129$. On the left we see the complete field dependence (for small field values the slow-roll approximation is inaccurate); the horizontal lines correspond to the experimental bounds to the quantity $n_s(k_{cmb})$, while the vertical line marks the CMB scale. On the right, the area around CMB scales is shown in greater detail, and the value of n_s looks compatible with the observational bounds.

Firstly, we considered models in which there is an exact inflection point, by imposing conditions (5.2.5) on the model parameters. We searched for parameters that reproduce the CMB data for $\mathcal{P}_\mathcal{R}$ and $n_s - 1$, and that also satisfy the condition $\delta_2 \lesssim -3$ (USR condition). To evaluate δ_2, we first solve numerically the Klein-Gordon equation, obtaining the field evolution as a function of the number of e-folds. We then calculate the parameter δ_1 using its definition, $\delta_1 = \frac{\mathrm{d}\,\sigma(N)/\mathrm{d}N}{\sigma(N)}$. Then, using (4.1.11) and (4.1.12), we find δ_2 as a function of δ_1:

$$\delta_2 = \frac{1}{\delta_1 h}(-\delta_1^2 h - 24(-2n_U + n_V)U^2h^2 + 12U\delta_1 h^2(3n_U(-n_U + n_V)U + h^2)$$

$$- \delta_1^3 h^4(n_U(2(n_U + n_{n_U} - 1) + n_V)U + h^2) + 2U\delta_1^2 h^2(6n_U^2(n_U + n_{n_U} + n_V - 1)U$$

$$+ (7n_U - n_V)h^2)/(4Uh(3n_U^2U + h^2))\,.$$

By numerically computing the power spectrum, we observe that, in the current framework, we cannot reach the required amplification of the power spectrum. To achieve a more efficient enhancement, we must add a small correction to the term $\sim h^6$ in order to create a quasi-inflection point in the Einstein frame. The correction will modify the potential in the following way:

$$V(h) = \frac{\lambda}{4}h^4(1 + (1+\epsilon)v_2h^2 + v_4h^4)\,. \tag{5.2.10}$$

By adding a small bump and tuning the parameter ϵ properly, we will see in the next section that the required 7 orders of magnitude of amplification can be achieved. We will

also evaluate the model in terms of the observables by calculating the relevant parameters (n_s and r) using expressions (4.3.9) and (4.3.10), as well as the PBH mass, and evaluating the results in light of recent experimental data.

5.2.1 Exploring the Higgs Inflation parameter space

We first present the results obtained considering the parameter λ to be the Higgs quartic self-coupling. We consider the reference value obtained from Standard Model theory:

$$\lambda = \frac{m_H^2}{2\,v^2}\,. \tag{5.2.11}$$

Considering the values of m_H and v obtained from combined ATLAS and CMS experiments [65], $m_H \simeq 125$ GeV and $v \simeq 246$ GeV, the Higgs quartic self-coupling value in the SM is $\lambda_{SM} \simeq 0.129$. With this value, we obtain a match to the CMB scales and a sufficiently large and negative parameter δ_1 for the following parameter choice:

$$u_2 = -10^{-6} \tag{5.2.12}$$

$$u_4 = 3.50752 \times 10^7 \tag{5.2.13}$$

$$h_0 = 0.0110917\,. \tag{5.2.14}$$

In this Higgs inflation model, the slow-roll phase occurs in the regime where the potential V is proportional to $\sim h^8$, it therefore requires a large value of the coefficient u_4 in order to flatten the potential $W = V/U^2$. While we have observed that the parameters u_4 and h_0 are highly tuned, the coefficient u_2 has to be small in modulo ($|u_2| \ll 1$) but we have observed that its precise value, as well as the sign, is not relevant for the model.

The estimated number of e-folds between CMB scales horizon exit and the inflection point is $\Delta N \simeq 39$ e-folds. In order to obtain an acceptable duration of inflation of about $50-60$ e-folds [66, 67], we selected a value of the parameter ϵ that allows for a sufficiently long USR period. The chosen value is:

$$\epsilon = 0.00227585\,. \tag{5.2.15}$$

With these parameters, we obtain that inflation lasts ~ 52 e-folds in total, and the scalar spectral index value is

$$n_s = 0.9494 \tag{5.2.16}$$

which is in fairly good agreement with the measured value. We can also calculate the

running of the scalar spectral index, $\alpha_s \equiv \frac{\mathrm{d}n_s}{\mathrm{d}lnk}$, for which we obtain the value

$$\alpha_s = -0.00127\,. \tag{5.2.17}$$

Experiments have estimated that the value of the running of n_s is $\alpha_s = -0.0041 \pm 0.0067$ [31], therefore this result lies within the acceptable bounds.

To evaluate the PBH mass, we use expression (3.1.10), that we report here:

$$M_{pbh}(N_{pbh}) \approx 7.7 \cdot 10^{17} e^{-2(N_{pbh}-N_{cmb})(1-\varepsilon_1)} \left(\frac{\gamma}{0.2}\right) \left(\frac{g_*(T_f)}{106.75}\right)^{-1/6} M_\odot\,. \tag{5.2.18}$$

Assuming a constant parameter ε_1, we consider the evolution of H between the time of PBH formation and CMB. The factor $e^{2(N_{pbh}-N_{cmb})\varepsilon_1}$ is then written as:

$$e^{2(N_{pbh}-N_{cmb})\varepsilon_1} = \frac{H_{cmb}^2}{H_{pbh}^2}\,. \tag{5.2.19}$$

We also assume $g_*(T_f) \sim 3.38$, $M_P = 1$ and choose an efficiency factor $\gamma \sim 0.015$ in order to obtain the following expression:

$$M_{pbh} = 1.058 \times 10^{17} \left(\frac{H_{cmb}^2}{H_{pbh}^2}\right) e^{-2(N_{pbh}-N_{cmb})}\, M_\odot\,. \tag{5.2.20}$$

Using (5.2.20), we obtain a mass of

$$M_{pbh} = 1.7617 \times 10^{-14} M_\odot\,. \tag{5.2.21}$$

Referencing the Figure (3.1), we can see that this value for M_{pbh} is included in window A. In this interval, the parameter f_{pbh} can take any value, which means that PBHs having this mass could potentially constitute the entire dark matter content in the present Universe. Such a large range for f_{pbh} is also indicative of this model being adaptable to multiple theories for PBH formation.

Below, in Fig. (5.7) we present a series of plots in which we show and comment the relevant functions and parameters, and how they change during inflation.

Let us now note that estimating the amplification with the analytical expression for the spectrum of scalar perturbations amplitudes in slow-roll approximation (4.3.4) fails to reproduce the correct model predictions. Indeed, using the result for the field evolution shown in Fig. (5.7c), we obtain the Figure (5.8) and the peak of the amplified spectrum does not reach the required value $\mathcal{P}_\mathcal{R} \simeq -2$, but in order to complete the analysis we have to look at the result for the numerical computation of the spectrum. The result is

Figure 5.7

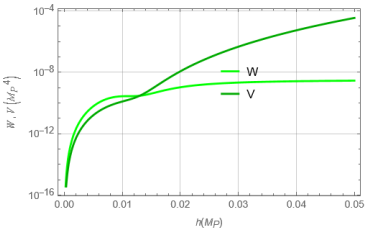

(a) In this plot we show the Jordan frame potential $V(h)$ and the Einstein frame potential $W(h)$ with $\epsilon = 0$. The inflection point is at $h_0 = 0.0110917$. In both frames the inflection point corresponds to a flatter region, which in the Einstein frame is exactly flat.

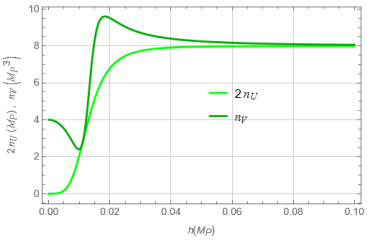

(b) One of the conditions for the inflection point is that the quantity $2n_U - n_V$ has to be zero. In this plot, we see that this is true in correspondence of h_0.

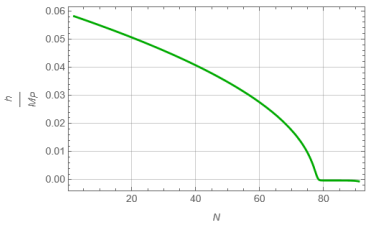

(c) In this plot, we look at the result of the numerical resolution of the Klein-Gordon equation. Comparing with the graph of δ_2, we observe that the USR regime, in which the field is nearly constant, starts where the dip in δ_2 is. The value of the field at this point is $h = h_0$.

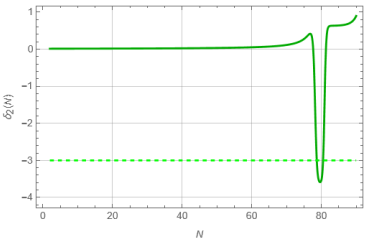

(d) This plot shows the variation of the exact parameter δ_2. The dip corresponds to the inflection point. The parameter δ_2 reaches the expected value of -3, meeting the condition for USR.

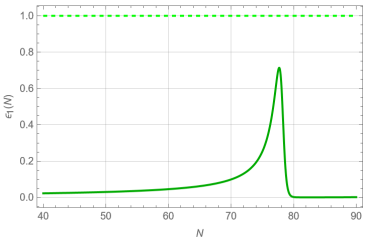

(e) The parameter ε_1 meets the fundamental constraint for inflation, $\varepsilon_1 \ll 1$, throughout all the period.

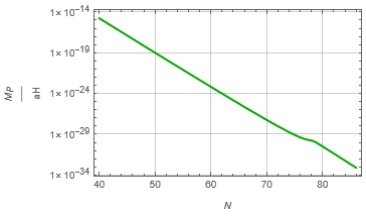

(f) In this plot, we see the variation of the Hubble radius $1/aH$, that shrinks during the inflation period.

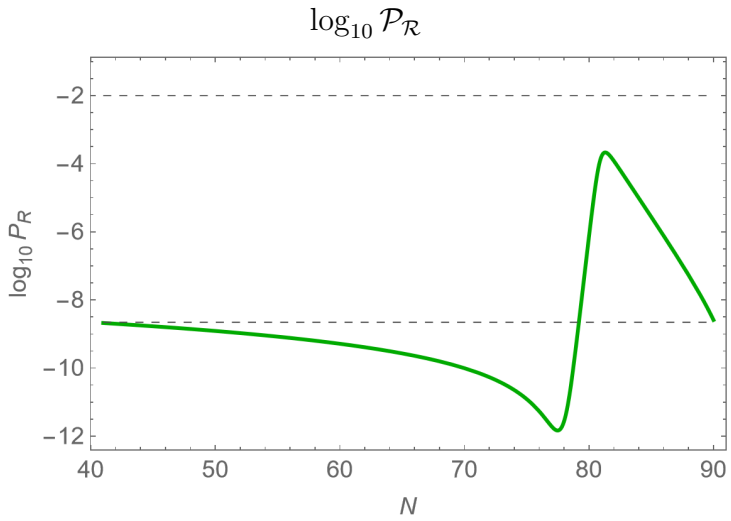

Figure 5.8: Logarithmic plot of amplitude spectrum of scalar perturbations for $\lambda = 0.129$. The green solid line is the spectrum, while the bottom dashed line is the value of $\mathcal{P}_{\mathcal{R}}$ at CMB scales, $\log_{10}\mathcal{P}_{\mathcal{R}cmb} = -8.66$.

shown in Figure (5.9).

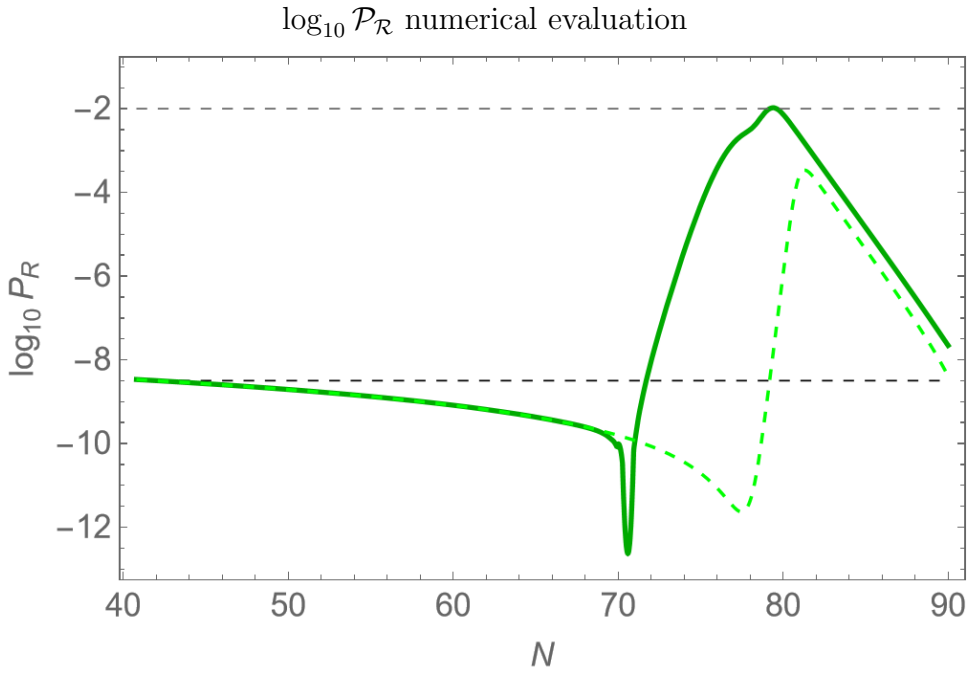

Figure 5.9: Logarithmic plot of the scalar spectrum $\mathcal{P}_{\mathcal{R}}$. The thick green line is the numerically evaluated spectrum, while the thinner line is the previously calculated analytical SR approximation. The horizontal dashed lines mark the value -2, which is a reference for sufficient amplifications, and -8.66, which is the value of $\mathcal{P}_{\mathcal{R}}$ at CMB scales.

In this plot, the previous estimate of the spectrum is in dashed green, while the exact numerical result is the thicker, darker green line. As we can see, the slow-roll approximation underestimates the amplification, and fails in the region between $N \sim 67$

and $N \sim 83$, which, comparing with Figures (5.7e) and (5.7d), corresponds to the interval in which the parameters δ_2 and ϵ_1 deviate from SR behavior. Again, the horizontal dashed lines mark the value -2, which is the goal, and -8.66, which is the value of $\log_{10}\mathcal{P}_\mathcal{R}$ at CMB scales. Let us note that, if the peak of the spectrum exceeds the value 10^{-2}, there is an overproduction of PBHs.

We also report the resulting scalar spectral index value

$$n_s = 0.9494 \tag{5.2.22}$$

and the tensor-to-scalar ratio value

$$r = 0.01133\,. \tag{5.2.23}$$

We conclude that this numerical estimate confirms the presence of an amplification of scalar perturbations that is sufficient to produce primordial black holes in a mass range which is within experimental bounds.

So far, we considered the Standard Model tree-level value for λ, but we can also take into account higher-order corrections, that depend on the Higgs mass and on masses of other particles in the SM, such as the top quark or the W gauge boson, which are also modified by corrections. This means that λ is associated to a range of possible values that is constantly evolving as the research progresses in looking for bounds for the SM parameters. We consider the results of the CMS collaboration presented in ref. [65] in 2023. In this review, the boundaries for the Higgs quartic self-coupling are presented in terms of the modifier

$$k_\lambda \equiv \frac{\lambda}{\lambda_{sm}} \tag{5.2.24}$$

which is the ratio between the coupling effective value λ after renormalization and the tree-level value λ_{sm}. The bounds are:

$$-1.24 \lesssim k_\lambda \lesssim 6.49\,. \tag{5.2.25}$$

This means that:

$$-0.16 \lesssim \lambda \lesssim 0.84\,. \tag{5.2.26}$$

What we can do now is to consider other values for the parameter λ that are inside this interval, and see how the model behaves and how much the model parameters are constrained.

In Figure (5.10), we plotted the resulting spectra for different values of λ, covering the range between 0.02 and 0.25. The numerical evaluation becomes problematic for values above this interval, however, we believe that it could be extended using more powerful

numerical computation techniques. Nonetheless, we can conclude that in the mentioned range, amplification for PBH production is in fact possible, with the right parameters choice.

$\log_{10} \mathcal{P}_{\mathcal{R}}$ numerical evaluation for different λ values

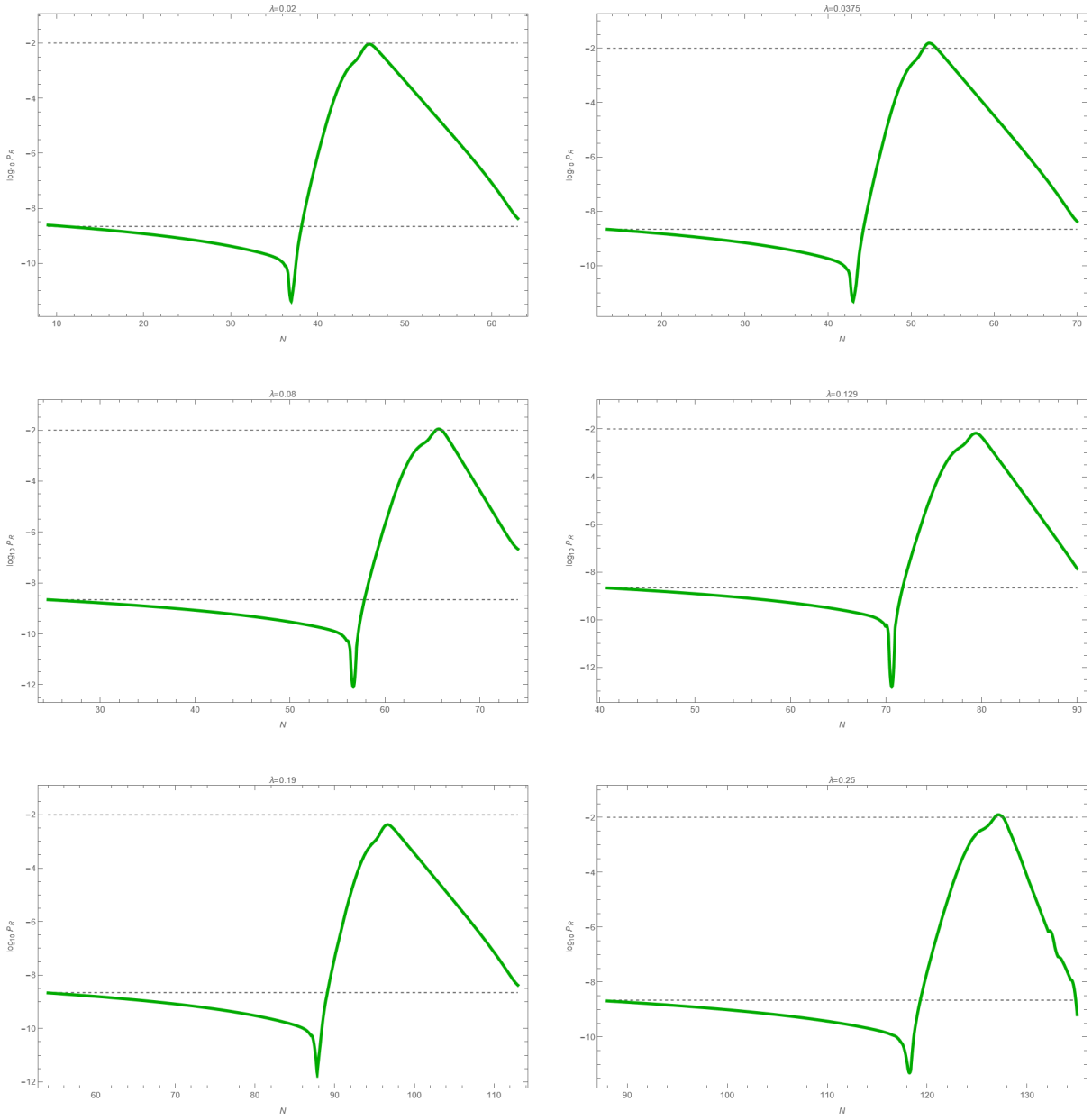

Figure 5.10: Logarithmic plots of spectrum amplitude for many values of λ. All the models are normalized to have starting amplitude corresponding to the CMB measure ($\log_{10}[\mathcal{P}_{\mathcal{R}}(k_{cmb})] = -8.66$), and both -2 and -8.66 are marked with a horizontal line. On the horizontal axis, the coordinate is always the number of e-folds, and the starting point is different in each case, as it depends on the number of e-folds that the system needs to stabilize itself in the slow-roll attractor dynamics, given certain initial conditions for the inflaton field. In each graph, the initial N coordinate is taken to be the CMB modes exit time for each case.

We gathered the results for PBH masses in table (5.1). The resulting values all lie in window A of Fig. (3.1). This window is the less constrained in terms of the PBH abundance β, meaning that those values for M_{pbh} could represent any fraction of dark matter. In table (5.2), we report all parameters for each studied model.

λ	PBH Mass $[M_\odot]$	n_s	r	α_s	N_{inf} $[N]$
0.0200	6.79×10^{-14}	0.9497	0.011	-0.0014	57.05
0.0250	5.26×10^{-14}	0.9501	0.011	-0.0013	56.58
0.0350	4.40×10^{-15}	0.9525	0.010	-0.0012	51.09
0.0375	6.07×10^{-15}	0.9514	0.011	-0.0013	66.08
0.0500	5.68×10^{-14}	0.9501	0.011	-0.0013	62.44
0.0600	9.12×10^{-14}	0.9504	0.011	-0.0013	60.53
0.0700	4.79×10^{-15}	0.9523	0.010	-0.0012	52.34
0.0800	9.24×10^{-17}	0.9541	0.009	-0.0011	53.86
0.1250	9.75×10^{-15}	0.9511	0.011	-0.0013	59.53
0.1290	1.71×10^{-14}	0.9511	0.011	-0.0013	51.39
0.1900	9.39×10^{-15}	0.9519	0.011	-0.0012	57.36
0.2300	1.71×10^{-16}	0.9526	0.010	-0.0012	60.66
0.2500	6.93×10^{-16}	0.9564	0.010	-0.0007	50.10
0.3500	5.35×10^{-15}	0.9520	0.010	-0.0012	55.39

Table 5.1: Results for PBH masses and cosmological parameters

λ	u_2	u_4	h_0
0.0200	-10^{-6}	5.01187×10^6	0.01819700
0.0250	-10^{-6}	6.30957×10^6	0.01717910
0.0350	-10^{-6}	1.00000×10^7	0.01513560
0.0375	-10^{-6}	1.00000×10^7	0.01531090
0.0500	-10^{-6}	1.25893×10^7	0.01445440
0.0600	-10^{-6}	1.58489×10^7	0.01348960
0.0700	-10^{-6}	1.99526×10^7	0.01273500
0.0800	-10^{-6}	2.51189×10^7	0.01202260
0.1250	-10^{-6}	3.23594×10^7	0.01145510
0.1290	-10^{-6}	3.50752×10^7	0.01109170
0.1900	-10^{-6}	5.01187×10^7	0.01023290
0.2300	-10^{-6}	6.30957×10^7	0.00977237
0.2500	-10^{-6}	7.94328×10^7	0.00891251
0.3500	-10^{-6}	1.00000×10^8	0.00851138

Table 5.2: List of studied parameters

In the graph (5.11), we show the results of table (5.1) in the parameter space (n_s, r). The blue region represents the joint constraints of Planck TT, TE, EE+lowE+lensing with BAO and BICEP2/Keck; the red and green region represent the Planck TT,TE,EE+lowE and Planck TT, TE, EE+lowE+lensing bounds respectively.

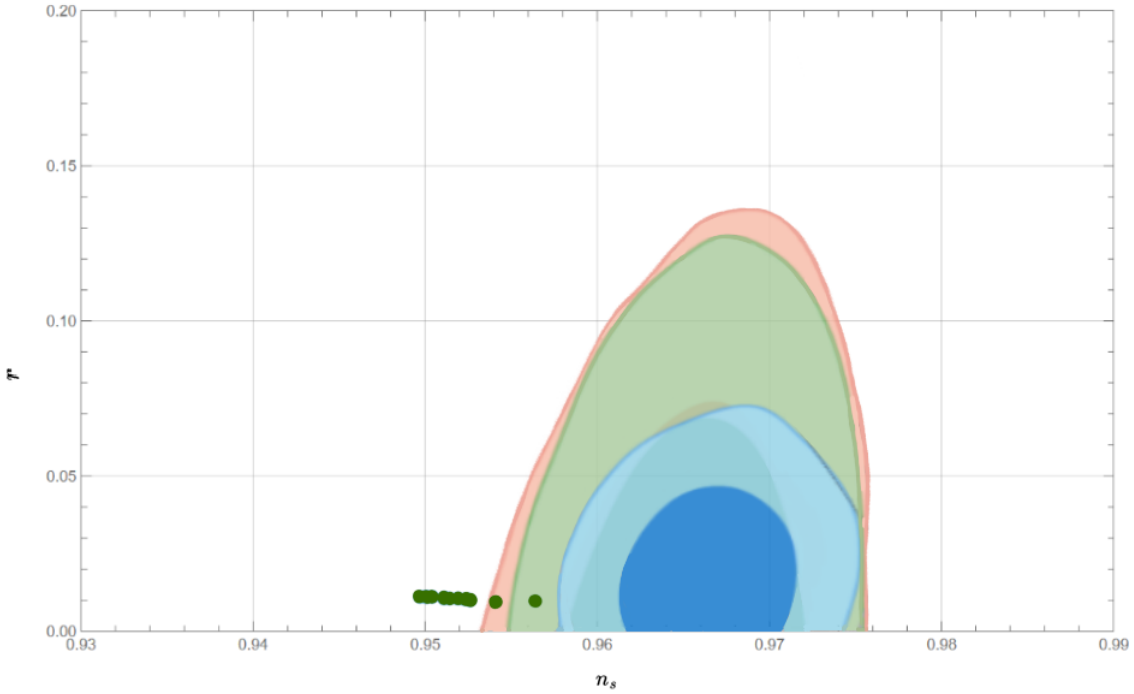

Figure 5.11

The points shown in the plot are compatible with the latest constraints imposed by the Planck experiment [64] within 3σ. Let us note that, considering a running scalar spectral index ($\mathrm{d}n_s/\mathrm{d}\ln k \neq 0$), the CMB observations favour smaller values of n_s compared to the constant case plotted in Fig. (5.11). This could reduce the tension between the model and the experimental bounds.

We also show the results of Table (5.1) in the plane (n_s, α_s) in Fig. (5.12). Results from Planck TT,TE,EE+lowE are shown in grey, Planck TT,TE,EE+lowE+lensing in red, and Planck TT,TE,EE+lowE+lensing+BAO in blue.

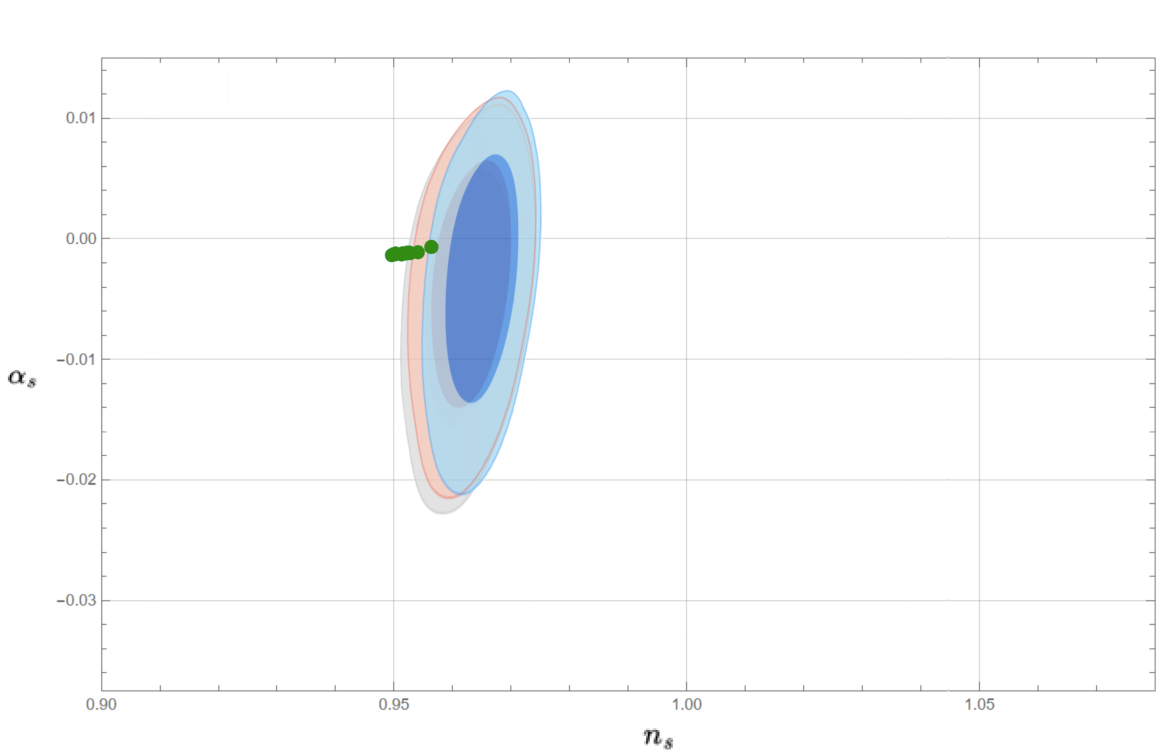

Figure 5.12

The values of the running α_s all lie within the acceptable bounds.

In conclusion, this analysis of Higgs inflation in the Jordan frame, including the study of ultra-slow-roll dynamics and its implications for primordial black hole (PBH) production, shows that the explored parameter space is compatible with current observational constraints. In particular, the predictions for the spectral index and the tensor-to-scalar ratio lie within the bounds established by Planck data, and the scenarios leading to power spectrum enhancement at small scales are capable of satisfying the necessary amplification conditions for PBH formation.

Conclusions

In this thesis we focused on the study of a particular inflationary scenario that includes a transient ultra–slow–roll phase induced by the presence of an inflection (or quasi–inflection) point in the inflaton potential. In particular, we studied a model in which the inflaton is identified with the Higgs field, since such an approach features a convenient framework that does not require the addition of any new scalar field beyond those already present in the Standard Model. In this context, the aim was to determine whether a modified Higgs inflation action could lead to the generation of a large enhancement of the curvature perturbation spectrum, sufficient to produce a phenomenologically relevant abundance of primordial black holes (PBHs) at the end of inflation.

In order to achieve this goal, we considered the Higgs inflation action supplemented by higher-order operators in the potential and in the non-minimal coupling. These operators do not affect the power spectrum at CMB scales, therefore they do not invalidate the predictions at those scales, which remain in agreement with current observations [31, 64]. However, the additional operators alter the shape of the potential, creating a sufficiently flat region that induces a transient ultra–slow–roll phase. Such a regime modifies the standard slow–roll dynamics, generating a strong amplification of the primordial power spectrum on scales that exit the Hubble radius during the ultra–slow–roll interval.

Within this extended theoretical framework, a new effective potential featuring a quasi-inflection point was constructed by introducing a small correction to term $\sim h^6$ in V. The resulting model was investigated numerically, analyzing the evolution of the background dynamics and the curvature perturbations for different choices of the model parameters. The parameters were first selected to reproduce the CMB observables in the initial slow-roll regime, and the parameter associated with the quasi-inflection point was chosen in order to obtain a peak amplitude of $\log_{10} \mathcal{P}_\mathcal{R} \sim -2$ (larger peak values would lead to an overproduction of PBHs). The explored parameter space range was based on the allowed range of the Higgs self-coupling λ in Higgs inflation [65]. Since higher-order renormalization corrections prevent the exact determination of λ, it is still reasonable to search within this interval in the context of Higgs inflation.

We have shown that, for a small region of parameter space, the perturbation spectrum exhibits an enhancement of approximately seven orders of magnitude relative to the

standard slow–roll prediction. This level of amplification is compatible with the value required for PBH formation and leads to the production of a non-negligible PBH population (Ω_{dm} depending on the PBHs mass). Moreover, the resulting PBH masses lie in a region of the mass spectrum that is not excluded by current bounds. We have also calculated the values of the main cosmological observables (n_s, r and α_s) and compared the results with the current relevant bounds.

Several open issues nevertheless remain. Firstly, the effective action considered in this work includes only a restricted number of higher-order operators. A complete assessment of the stability of the model with respect to radiative corrections has not been performed and requires further investigation. Secondly, the present analysis has focused exclusively on the linear perturbation regime. A study of the associated non-Gaussianities is necessary in order to determine whether higher-order statistical moments of the perturbation spectrum might place additional constraints on the model. Furthermore, a detailed study of the reheating phase could help in determining more precisely the PBHs masses, although we expect the results not being very different from the standard Higgs inflation results. It also has been shown that gravitational–wave observatories such as NANOGrav [68] and future detectors may probe the stochastic gravitational-wave background associated with the amplified perturbations, offering complementary ways to test this class of inflationary models.

Appendix A

Second-order action of scalar perturbations

Following ref. [15], in this section we derive the second-order action to describe the dynamics of scalar perturbations in FLRW spacetime.

We start by considering the background metric (1.1.1) with $k = 0$ (flat) in the Arnowitt-Deser-Misner (ADM) formalism [69]:

$$ds^2 = -n^2 dt^2 + g_{ij}(dx^i + N^i dt)(dx^j + N^j dt)\,. \tag{A.0.1}$$

In this formalism, the metric g_{ij} covers only the spatial slicing, while the local parametrization of the coordinates is described by four functions: the lapse function $n(\mathbf{x})$ and the shift functions $N_i(\mathbf{x})$. We want to treat these four functions as Lagrange multipliers and find their algebraic equations of motion. The lapse and shift functions are not physical degrees of freedom, they instead represent the gauge symmetry of the FLRW spacetime.

Using the ADM formalism, the action (1.7.1) becomes

$$S_{ADM} = \frac{1}{2}\int d^4x\sqrt{-g}[nR^{(3)} - 2nV + n^{-1}(E_{ij}E^{ij} - (E^i_i)^2) + \\ + n^{-1}(\dot{\phi} - N^i\partial_i\phi)^2 - ng^{ij}\partial_i\phi\partial_j\phi - 2V] \tag{A.0.2}$$

where we define

$$E_{ij} \equiv \frac{1}{2}(\dot{g}_{ij} - \nabla_i N_j - \nabla_j N_i)\,. \tag{A.0.3}$$

After imposing the conditions for the comoving gauge (2.1.26), by varying the action

(A.0.2) we find two constraint equations:

$$\nabla_i[n^{-1}(E^i_j - \delta^i_j E)] = 0 \tag{A.0.4}$$

$$R^{(3)} - 2V - n^{-2}(E_{ij}E^{ij} - E^2) - n^{-2}\dot{\phi}^2 = 0\,. \tag{A.0.5}$$

To solve these equations, we decompose the shift vector introducing one irrotational part and one incompressible part:

$$N_i \equiv \psi_{,i} + \tilde{N}_i\,, \quad \tilde{N}_{i,i} = 0 \tag{A.0.6}$$

and redefine the lapse function as

$$n \equiv 1 + \alpha\,. \tag{A.0.7}$$

Then, we expand ψ, $\tilde{N}_i$ and α in powers of $\mathcal{R}$:

$$\psi = \psi_1 + \psi_2 + \mathcal{O}(\mathcal{R}^3)$$

$$\tilde{N}_i = \tilde{N}^{(1)}_i + \tilde{N}^{(2)}_i + \mathcal{O}(\mathcal{R}^3)$$

$$\alpha = \alpha_1 + \alpha_2 + \mathcal{O}(\mathcal{R}^3)$$

where each term represents one order in $\mathcal{R}$. We can write the constraint equations in terms of these terms and then solve order by order in $\mathcal{R}$. To obtain the second-order action, it is sufficient to solve the constraint equations at first order. The equation (A.0.5) implies

$$\alpha_1 = \frac{\dot{\mathcal{R}}}{H}\,, \quad \partial^2 \tilde{N}^{(1)}_i = 0\,. \tag{A.0.8}$$

The parameters $\tilde{N}^{(1)}_i$ can be set to zero by choosing the boundary conditions accordingly. Equation (A.0.4) implies

$$\psi_1 = -\frac{\mathcal{R}}{H} + \frac{a^2}{2H}\left(\frac{V_{,\phi}}{V}\right)^2 \partial^{-2}\dot{\mathcal{R}}\,. \tag{A.0.9}$$

Substituting the first-order solutions for n and N_i into the action (A.0.2), we obtain the second-order action for $\mathcal{R}$:

$$\mathcal{S}^{(2)}_{\mathcal{R}} = \frac{1}{2}\int d^4x\, a^3 \frac{\dot{\phi}^2}{H^2}\left[\dot{\mathcal{R}}^2 - a^{-2}(\partial_i \mathcal{R})^2\right]\,. \tag{A.0.10}$$

Appendix B

Analytical modes evolution in non-slow-roll phases

In this appendix, following ref. [70], we describe a technique that can be used to find an analytic form for the power spectrum evolution from matching the initial SR, intermediate USR and final SR periods. Although the result is still approximate, it can provide contact between numerical results and an analytical formalism. We assume that, in these intermediate phases, the SR parameters are constant.

We start from the definition of the pump field z (2.2.3), and, differentiating with respect to conformal time, the term z''/z in the Mukhanov-Sasaki equation becomes:

$$\frac{z''}{z} = (aH)^2 \left(2 - \varepsilon_1 + \frac{3}{2}\eta + \frac{1}{4}\eta^2 - \frac{1}{2}\varepsilon_1\eta + \frac{1}{2}\frac{\dot{\eta}}{H}\right) \tag{B.0.1}$$

where the parameter η is:

$$\eta \equiv 2\left(\varepsilon_1 + \frac{\ddot{\phi}}{\dot{\phi}H}\right) . \tag{B.0.2}$$

The slow-roll regime corresponds to $\eta \ll 1$ (we approximate to $\eta \simeq 0$), while in the ultra-slow-roll regime $\eta \simeq -6$, because $\varepsilon_1 \ll 1$ and, from Eq. (2.4.5), $\frac{\ddot{\phi}}{\dot{\phi}H} \simeq -3$.

Assuming $\varepsilon_1 \ll 1$, we can write Eq. (2.2.4) as:

$$v_k'' + \left(k^2 - \frac{\nu^2 - 1/4}{\tau^2}\right) v_k = 0 \tag{B.0.3}$$

where the new parameter is

$$\nu \equiv \frac{9}{4} + \frac{3}{2}\eta + \frac{1}{4}\eta^2 + \frac{\dot{\eta}}{2H} . \tag{B.0.4}$$

The solutions to Eq. (B.0.3) are:

$$v_k = \frac{\sqrt{\pi}}{2} e^{i(\nu+1/2)\frac{\pi}{2}} \sqrt{-\tau} H_\nu^{(1)}(-k\tau) \tag{B.0.5}$$

and their complex conjugates, where $H_\nu^{(1)}(-k\tau)$ is the Hankel function of the first kind. For the slow-roll phase and ultra-slow-roll phase, we find respectively $\nu = 3/2$ and $\nu = -3/2$. Now, we can write the solution $\mathcal{R}_\parallel = v/z$ for the modes equation in each phase and match them with appropriate boundary conditions:

1. At the beginning we have a slow-roll phase ($\eta = 0$). The mode functions for the curvature perturbations are given by:

$$\mathcal{R}_k^{(1)} = i\frac{H}{M_P}\frac{1}{\sqrt{4\varepsilon_1 k^3}}\left[c(1+ik\tau)e^{-ik\tau} - s(1-ik\tau)e^{ik\tau}\right] . \tag{B.0.6}$$

   Implementing the Bunch-Davies vacuum condition at early conformal time, (B.0.6) becomes:

$$\mathcal{R}_k^{(1)} = i\frac{H}{M_P}\frac{e^{-ik\tau}}{\sqrt{4\varepsilon_1}k^3}(1+ik\tau) . \tag{B.0.7}$$

   This is the solution that we found in chapter (2).

2. To find $\mathcal{R}_\parallel$ in the ultra-slow-roll period, we write the parameter ε_1 as

$$\varepsilon_1^{(usr)} = \varepsilon_1 \left(\frac{a(\tau_1)}{a(\tau)}\right)^6 = \varepsilon_1 \left(\frac{\tau_1}{\tau}\right)^6 \tag{B.0.8}$$

   where τ_1 is the time of transition between SR and USR, and the second equality comes from $aH = -1/\tau$, considering that H is constant during inflation. Notation-wise, from this point forward the symbol ε_1 will refer to the SR parameter in the first slow-roll phase.

   The canonically normalized mode functions during the USR phase are:

$$\mathcal{R}_k^{(2)} = i\frac{H}{M_P}\frac{(\tau_1/\tau)^3}{\sqrt{4\varepsilon_1 k^3}}\left[c_1(1+ik\tau)e^{-ik\tau} - s_1(1-ik\tau)e^{ik\tau}\right] . \tag{B.0.9}$$

   The coefficients c_1 and s_1 are found by matching with the initial SR phase. The matching conditions are given by the Israel junction conditions:

$$[\mathcal{R}_k]_\pm = 0 \tag{B.0.10}$$

$$[z^2 \mathcal{R}'_k]_\pm = 0 \tag{B.0.11}$$

The first corresponds to the requirement that the metric be continuous across the transition, and the second follows from Eq. (2.2.2), which implies:

$$(z^2\mathcal{R}_k') = -z^2k^2\mathcal{R}_k\,. \tag{B.0.12}$$

Integrating the above expression over an infinitesimal interval around the transition, and recalling that $\mathcal{R}_\parallel$ and z^2 are continuous, the result is (B.0.11).

The two junction conditions result in the following two equations:

$$(1+ik\tau_1)e^{-ik\tau 1} = c_1(1+ik\tau_1)e^{-ik\tau_1} - s_1(1-ik\tau_1)e^{ik\tau_1}\,, \tag{B.0.13}$$

$$k^2\tau_1 e^{-ik\tau_1} = c_1 e^{-ik\tau_1}\left(k^2\tau_1 - \frac{3}{\tau_1}(1+ik\tau_2)\right) - s_1 e^{ik\tau_1}\left(k^2\tau_1 - \frac{3}{\tau_1}(1-ik\tau_2)\right)\,. \tag{B.0.14}$$

Solving these, the results for the two coefficients are:

$$s_1 = \frac{3\,i\,e^{-2ik\tau_1}}{2(k\tau_1)^3}(1+ik\tau_1)^2 \tag{B.0.15}$$

$$c_1 = 1 + \frac{3\,i\,(1+k^2\tau_1^2)}{2(k\tau_1)^3} \tag{B.0.16}$$

3. We now consider a second transition to the final SR phase, in which the slow-roll parameter ε_1 is the constant

$$\varepsilon_1^{(sr,2)} = \varepsilon_1\left(\frac{\tau_2}{\tau_1}\right)^6 \tag{B.0.17}$$

where τ_2 is the conformal time at the end of the USR period. The mode functions are:

$$\mathcal{R}_k^{(3)} = i\frac{H}{M_P}\frac{(\tau_1/\tau_2)^3}{\sqrt{4\varepsilon_1 k^3}}\left[c_2(1+ik\tau)e^{-ik\tau} - s_2(1-ik\tau)e^{ik\tau}\right]\,. \tag{B.0.18}$$

By applying the junction conditions (B.0.10) and (B.0.11), we find, for the coefficients c_2 and s_2:

$$c_2 = -\frac{1}{4k^6\tau_1^3\tau_2^3}[9\, e^{2ik(\tau_2-\tau_1)}\,(k\tau_1 - i)^2(k\tau_2 + i)^2 - \\ - (k^2\tau_1^2\,(2k\tau_1 + 3i)\, +\, 3i)\,(k^2\tau_2^2(2k\tau_2 - 3i)\, -\, 3i)] \quad \text{(B.0.19)}$$

$$s_2 = \frac{e^{-2ik(\tau_1+\tau_2)}}{4k^6\tau_1^3\tau_2^3}[3\, e^{2ik\tau_2}(3 + k^2\tau_2^2(3 - 2ik\tau_2))\,(k\tau_1 - i)^2 + \\ + 3i\, e^{2ik\tau_1}\,(k^2\tau_1^2(2k\tau_1 + 3i)\, +\, 3i)\,(k\tau_2 - i)^2] \quad \text{(B.0.20)}$$

The power spectrum for the curvature perturbation at late times is then (see (2.1.46)):

$$\mathcal{P}_\mathcal{R} = \frac{H^2 e^{6N_{usr}}}{8\pi^2 M_P^2 \varepsilon_1}(c_2^* c_2 + s_2^* s_2 - s_2^* c_2 - s_2 c_2^*) \quad \text{(B.0.21)}$$

and it differs from the power spectrum in pure slow-roll regime by a factor

$$e^{6N_{usr}}\,(c_2^* c_2 + s_2^* s_2 - s_2^* c_2 - s_2 c_2^*) \quad \text{(B.0.22)}$$

that depends on the wavelength k and on the conformal time at the start (τ_1) and at the end (τ_2) of USR. This three-phase matching is approximate, many short intermediate phases of constant η should be considered in order to improve the accuracy. For example, it would be realistic to add an intermediate phase where $\eta = -2$, or with positive η at the beginning of the transient phase.

Appendix C

Numerical resolution of Mukhanov-Sasaki equation

In this section, we describe the method that we used for the numerical resolution of the Mukhanov-Sasaki equation.

Starting from Eq. (2.2.4), that we report here:

$$\ddot{v_k} + \left(k^2 - \frac{\ddot{z}}{z}\right) v_k = 0 \,. \tag{C.0.1}$$

This equation can be rewritten as a harmonic oscillator equation of motion:

$$\ddot{v_k} + \omega^2 v_k = 0 \tag{C.0.2}$$

where we defined

$$\omega^2 \equiv k^2 - \ddot{z}/z \tag{C.0.3}$$

which, because of the term $\ddot{z}/z$, is a time-dependent frequency. As initial conditions, we want to implement the Bunch-Davies vacuum conditions (2.2.7), that we also report here:

$$v_k(\tau_0) = \frac{1}{\sqrt{2k}} \,, \quad \dot{v}_k(\tau_0) = -i\sqrt{\frac{k}{2}} \,. \tag{C.0.4}$$

The Mukhanov-Sasaki equation with Bunch-Davies initial conditions is a rather cumbersome equation to treat, as the solution is complex and highly oscillating. Moreover, the physical quantity we need to calculate from its physical solutions is real and proportional to $|v_k|^2$. To solve (2.2.4) it in a more efficient way, we first note that, given its identification with a time-dependent harmonic oscillator, the modulo of v_k is related to a variable ρ, called Pinney variable. This quantity is the solution of the Ermakov-Pinney

equation:

$$\ddot{\rho} + \omega^2 \rho = \frac{1}{\rho^3} \,. \tag{C.0.5}$$

Indeed, if $v_k = Ae^{i\theta}$, then (C.0.2) is:

$$\ddot{A}e^{i\theta} + 2i\dot{A}\dot{\theta}e^{i\theta} + iA\ddot{\theta}e^{i\theta} - A\dot{\theta}^2 e^{i\theta} + \omega^2 A e^{i\theta} = 0 \,. \tag{C.0.6}$$

Once the phase is simplified, one finds:

$$\ddot{A} + 2i\dot{A}\dot{\theta} + iA\ddot{\theta} - A\dot{\theta}^2 + A\omega^2 = 0 \,. \tag{C.0.7}$$

The real and imaginary parts of this last equation lead to two independent, real equations:

$$\begin{cases} \ddot{A} - A\dot{\theta}^2 + A\omega^2 = 0 \\ 2\dot{A}\dot{\theta} + A\ddot{\theta} = 0 \,. \end{cases} \tag{C.0.8}$$

The second equation can be solved for $\dot{\theta}$:

$$\frac{\ddot{\theta}}{\dot{\theta}} = -2\frac{\dot{A}}{A} \quad \rightarrow \quad \ln\frac{\dot{\theta}}{\dot{\theta}_0} = \ln\frac{A_0^2}{A^2} \quad \rightarrow \quad \dot{\theta} = \frac{C_0}{A^2} \tag{C.0.9}$$

where $C_0 = A_0^2\,\dot{\theta}_0$. Substituting this result into the first equation gives the Pinney equation:

$$\ddot{A} - \frac{C_0^2}{A^3} + A\omega^2 = 0 \,. \tag{C.0.10}$$

This result comes also from the theory of invariants, developed by Lewis and Riesenfeld [71]. For the time-dependent harmonic oscillator, one can define the following invariant operator:

$$I = \frac{1}{2}((\rho \cdot p - \dot{\rho} \cdot x)^2 + (x/\rho)^2) \tag{C.0.11}$$

where x is the variable, p is the momentum and ρ is the Pinney variable. Eigenstates of the non-hermitian Hamiltonian operator can be expressed, with a difference in phase, as eigenstates of the invariant operator I.

Once we find the solution to Eq. (C.0.5), we can write the power spectrum as:

$$\mathcal{P}_\mathcal{R} = \frac{k^3}{2\pi^2}|v_k^2| \quad \longrightarrow \quad \mathcal{P}_\mathcal{R} = \frac{k^3}{2\pi^2}\left|\frac{\rho^2}{2}\right| \,. \tag{C.0.12}$$

As the Pinney equation is quite complex to solve, because of its non-linearity, we consider a general solution of the Pinney equation written in terms of two independent

solutions of the associated homogeneous equation:

$$\ddot{\rho} + \omega^2 \rho = 0 \tag{C.0.13}$$

which has the same form of the Mukhanov-Sasaki equation but is real.

Let x and y be two independent solutions; then, a solution to (C.0.5) is

$$\rho = \sqrt{x^2 + \frac{y^2}{W^2}} \tag{C.0.14}$$

where $W = \dot{x}y - x\dot{y}$ is their Wronskian (constant).

As initial conditions for x and y, we choose

$$y(\tau_0) = 0\,, \quad \dot{y}(\tau_0) = A_\tau \tag{C.0.15}$$

for y, and

$$x(\tau_0) = \rho_0\,, \quad \dot{x}(\tau_0) = \dot{\rho}_0 \tag{C.0.16}$$

for x. A_τ is arbitrary, while the constant $\rho_0/\sqrt{2}$ is the modulo of the Bunch-Davies solution. This set of real initial conditions allows for a more efficient numerical resolution of Eq. (C.0.13). By setting the initial conditions (C.0.15) and (C.0.16), we recover the Bunch-Davies initial conditions for v_k.

We want to solve the Mukhanov-Sasaki equation with N as the independent variable. To do so, we switch variables in the terms that contain derivatives with respect to conformal time, using:

$$\frac{\mathrm{d}}{\mathrm{d}\tau} = H\frac{\mathrm{d}}{\mathrm{d}N} \quad \rightarrow \quad \frac{\mathrm{d}^2}{\mathrm{d}\tau^2} = \frac{\mathrm{d}^2}{\mathrm{d}N^2} + (1-\varepsilon_1)\frac{\mathrm{d}}{\mathrm{d}N}\,. \tag{C.0.17}$$

The first term in (2.2.4) becomes:

$$\ddot{v}_k = v_k'' + (1-\varepsilon_1)v_k' \tag{C.0.18}$$

and the term $\ddot{z}/z$ becomes:

$$\frac{\ddot{z}}{z} = \frac{z''}{z} + (1-\varepsilon_1)\frac{z'}{z} \tag{C.0.19}$$

where the prime denotes the derivative with respect to N.

The Wronskian, calculated in N_0, is:

$$W = -\rho_0 \cdot \dot{y}(\tau_0) = -\rho_0 \cdot A_N \cdot H(N_0) \tag{C.0.20}$$

where the constant $A_N = y'(N_0)$ is the arbitrary initial condition if N is considered as the independent variable.

Bibliography

[1] A. H. Guth. "The Inflationary Universe: A Possible Solution to the Horizon and Flatness Problems". In: *Phys.Rev.D 23* (1981).

[2] A. D. Linde. "A New Inflationary Universe Scenario: A Possible Solution of the Horizon, Flatness, Homogeneity, Isotropy and Primordial Monopole Problems". In: *Phys.Lett.B 108* (1981).

[3] S. W. Hawking B. J. Carr. "Black Holes in The Early Universe". In: *Monthly Notices of the Royal Astronomical Society, Volume 168, Issue 2, August 1974, Pages 399–415* (1974).

[4] B. J. Carr. "The Primordial Black Hole Mass Spectrum". In: *Astrophysical Journal, vol. 201, pt. 1, p. 1-19* (1975).

[5] M. Shaposhnikov F. Bezrukov. *The Standard Model Higgs Boson as the Inflaton*. 2007. arXiv: 0710.3755v2.

[6] F. Bezrukov. *The Higgs Field as an Inflaton*. 2013. arXiv: 1307.0708v2.

[7] G. Hinsaw et al. *Nine-Year Wilkinson Microwave Anisotropy Probe (WMAP) Observations: Cosmological Parameter Results*. 2013. arXiv: 1212.5226v3.

[8] R.W. Wilson A.A. Penzias. "A Measurement of Excess Antenna Temperature at 4080 Mc/s". In: *The Astrophysical Journal, 142* (1965).

[9] D. Baumann. *Cosmology*. Cambridge University Press, 2022.

[10] A. D. Linde. "Chaotic Inflation". In: *Phys.Lett.B 129, pages 177-181* (1983).

[11] A. V. Olinto K. Freese J. A. Frieman. "Natural inflation with pseudo Nambu-Goldstone bosons". In: *Phys. Rev. Lett. 65, 3233* (1990).

[12] A. Linde. "Hybrid Inflation". In: *Phys. Rev. D 49, page 748* (1994).

[13] G. Tasinato O. Ozsoy. *Inflation and Primordial Black Holes*. 2023. arXiv: 2301.03600v3.

[14] V. Mukhanov. *Physical Foundations of Cosmology*. Cambridge University Press, 2005.

[15] D. Baumann. *Inflation*. 2009. arXiv: 0907.5424v2.

[16] A. Riotto. *Inflation and the Theory of Cosmological Perturbations*. 2017. arXiv: 0210162v2.

[17] J. M. Bardeen. "Gauge-Invariant Cosmological Perturbations". In: *Phys.Rev.D 22* (1980).

[18] J. Maldacena. *Non-Gaussian Features of Primordial Fluctuations in Single-Field Inflationary Models*. 2005. arXiv: 0210603v5.

[19] P. C. W. Davies T. S. Bunch. "Quantum Field Theory in De Sitte Space: Renormalization by Point-Splitting". In: *Proc. R. Soc. Lond. A 360 117–134* (1978).

[20] W. Hu H. Motohashi. *Primordial Black Holes and Slow-Roll Violation*. 2017. arXiv: 1706.06784.

[21] S. M. Leach et al. *Enhancement of superhorizon scale inflationary curvature perturbations*. 2001. arXiv: 0101406v2.

[22] G. Tasinato. *An Analytic Approach to Non-Slow-Roll Inflation*. 2021. arXiv: 2012.02518v3.

[23] W. H. Kinney. *Horizon Crossing and Inflation With Large η*. 2005. arXiv: 0503017v3.

[24] J. Yokoyama H. Motohashi A. A. Starobinsky. *Inflation with a Constant Rate of Roll*. 2008. arXiv: 1411.5021v3.

[25] VIRGO Collaboration LIGO Scientific Collaboration. *Observation of Gravitational Waves from a Binary Black Hole Merger*. 2016. arXiv: 1602.03837.

[26] A. Escrivà. *Primordial Black Hole Formation from Spherically Symmetric Hydrodynamical Pertutbations: a Review*. 2022. arXiv: 2111.12693v3.

[27] M. Sasaki M. Shibata. *Black Hole Formation in the Friedmann Universe: Formulation and Computation in Numerical Relativity*. 1999. arXiv: 9905064v1.

[28] I. Musco. *Threshold for primordial black holes: Dependence on the shape of the cosmological perturbations*. 2019. arXiv: 1809.02127.

[29] R. K. Sheth A. Escrivà C. Germani. *Analytical Thresholds for Black Hole Formation in General Cosmological Backgrounds*. 2020. arXiv: 2007.05564v2.

[30] R. K. Sheth A. Escrivà C. Germani. *A Universal Threshold for Primordial Black Hole Formation*. 2020. arXiv: 1907.13311.

[31] Planck Collaboration. *Planck 2018 Results VI: Cosmological Parameters*. 2007. arXiv: 1807.06209.

[32] P. Schechter W. H. Press. "Formation of Galaxies and Clusters of Galaxies by Self-Similar Gravitational Condensation". In: *Astrophysical Journal, Vol. 187, pp. 425-438* (1974).

[33] M. Sasaki et al. *Primordial Black Holes - Perspectives in Gravitational Wave Astronomy*. 2018. arXiv: 1801.05235.

[34] F. Kuhnel B. Carr. *Primordial Black Holes as Dark Matter: Recent Developments*. 2020. arXiv: 2006.02838v3.

[35] B. J. Carr et al. "New Cosmological Constraints on Primordial Black Holes". In: *Physical Review D* (2010).

[36] M. Cirelli M. Boudaud. *Voyager 1 e± Further Constrain Primordial Black Holes as Dark Matter*. 2018. arXiv: 1807.03075.

[37] T. Slatyer R. Laha J. Munoz. *INTEGRAL constraints on primordial black holes and particle dark matter*. 2020. arXiv: 2004.00627.

[38] C. Man Lee M. Ho Chan. *Constraining Primordial Black Hole Fraction at the Galactic Centre using radio observational data*. 2020. arXiv: 2007.05677.

[39] A. Kirillov K. Belotsky. *Primordial black holes with mass 10^16 10^17 g and reionization of the Universe*. 2015. arXiv: 1409.8601.

[40] H. Niikura et al. *Microlensing constraints on primordial black holes with the Subaru/HSC Andromeda observation*. 2017. arXiv: 1701.02151.

[41] U. Seljak M. Zumalacarregui. *Limits on stellar-mass compact objects as dark matter from gravitational lensing of type Ia supernovae*. 2018. arXiv: 1712.02240.

[42] E. Mediavilla et al. *Microlensing-Based Estimate of the Mass Fraction in Compact Objects in Lens*. 2009. arXiv: 0910.3645.

[43] P. N. Wilkinson et al. *Limits on the cosmological abundance of supermassive compact objects from a search for multiple imaging in compact radio sources*. 2001. arXiv: 0101328.

[44] R. Turolla M. Roncadelli A. Treves. *Primordial black holes are again on the limelight*. 2009. arXiv: 0901.1093.

[45] M. Sakellariadou B. J. Carr. "Dynamical Constraints on Dark Matter in Compact Objects". In: *The Astrophysical Journal, Volume 516, Issue 1, pp. 195-220* (1999).

[46] B. J. Carr. "Pregalactic black hole accretion and the thermal history of the universe". In: *Monthly Notices of the Royal Astronomical Society 194, 639-668* (1981).

[47] M. Ricotti K. Mack J. Ostriker. *Growth of structure seeded by primordial black holes*. 2007. arXiv: astro-ph/0608642.

[48] M. Ricotti K. Mack J. Ostriker. *Effect of Primordial Black Holes on the Cosmic Microwave Background and Cosmological Parameter Estimates*. 2007. arXiv: 0709.0524.

[49] A. Kusenko Y. Inoue. *New X-ray bound on density of primordial black holes*. 2017. arXiv: 1705.00791.

[50] Philip Lu et al. *Constraining Primordial Black Holes with Dwarf Galaxy Heating*. 2020. arXiv: 2007.02213.

[51] H. Veermäe M. Raidal V. Vaskonen. *Gravitational Waves from Primordial Black Hole Mergers*. 2017. arXiv: 1707.01480.

[52] M. Raidal et al. *Formation and Evolution of Primordial Black Hole Binaries in the Early Universe*. 2019. arXiv: 1812.01930.

[53] H. Veermäe V. Vaskonen. *Lower bound on the primordial black hole merger rate*. 2019. arXiv: 1908.09752.

[54] Q. Huang Z. Chen C. Yuan. *Pulsar Timing Array Constraints on Primordial Black Holes with NANOGrav 11-Year Data Set*. 2019. arXiv: 1910.12239.

[55] M. Taoso G. Ballesteros P. D. Serpico. *On the merger rate of primordial black holes: effects of nearest neighbours distribution and clustering*. 2018. arXiv: 1807.02084.

[56] J. Silk P. Gondolo. *Dark matter annihilation at the galactic center*. 1999. arXiv: 9906391.

[57] F. Kuhnel B. Carr. *Primordial Black Holes as Dark Matter: Recent Developments*. 2020. arXiv: 2006.02838.

[58] B. J. Carr et al. "Primordial black hole constraints for extended mass functions". In: *Phys. Rev. D 96, 023514* (2017).

[59] K. Freese F. Kuhnel. *Constraints on Primordial Black Holes with Extended Mass Functions*. 2017. arXiv: 1701.07223.

[60] J. Garca-Bellido J. Ezquiaga and E. Morales. *Primordial Black Hole Production in Critical Higgs Inflation*. 2017. arXiv: 1705.04861v3.

[61] J. Rubio. *Higgs Inflation*. 2018. arXiv: 1807.02376v3.

[62] M. Shaposhnikov F. Bezrukov. *Higgs Inflation at the Critical Point*. 2014. arXiv: 1403.6078v2.

[63] D. Buttazzo et al. *Investigating the Near-Criticality of the Higgs Boson*. 2013. arXiv: 1307.3536.

[64] Planck Collaboration. *Planck 2018 results. X. Constraints on inflation*. 2018. arXiv: 1807.06211v2.

[65] CMS Collaboration. *A portrait of the Higgs boson by the CMS experiment ten years after the discovery*. 2022. arXiv: 2207.00043v3.

[66] S. Leach A. Liddle. "How long before the end of inflation were observable perturbations produced?" In: *Phys. Rev. D 68, 103503* (2003).

[67] G. Germàn et al. "Model independent bounds for the number of efolds during the evolution of the universe". In: *Journal of Cosmology and Astroparticle Physics, Volume 2023* (2023).

[68] G. Agazie et al. "The NANOGrav 15 yr Data Set: Evidence for a Gravitational-wave Background". In: *The Astrophysical Journal Letters, Volume 951, Number 1* (2023).

[69] C. W. Misner R. Arnowitt S. Deser. *The Dynamics of General Relativity*. 1962. arXiv: 0405109v1.

[70] S. P. Patil C. T. Byrnes P. S. Cole. *Steepest Growth of The Power Spectrum and Primordial Black Holes*. 2019. arXiv: 1811.11158v3.

[71] W. B. Riesenfeld H. R. Lewis. "An Exact Quantum Theory of the Time-Dependent Harmonic Oscillator and of a Charged Particle in a Time-Dependent Electromagnetic Field". In: *J. Math. Phys. 10, 1458–1473* (1969).